Analysis of Colour Channel Coupling from a Physics-based Viewpoint: Application to Colour Edge Detection

Alberto Ortiz * , Gabriel Oliver

University of the Balearic Islands, Dept. of Mathematics and Computer Science, Palma de Mallorca (SPAIN)

Abstract

The Dichromatic Reflection Model (DRM) introduced by Shafer in 1985 is surely the physics-based model of image formation most referenced in publications describing research in physics-based vision. A preliminary analysis of this model derives in the conclusion that colour channels keep coupled by the reflectance of objects surface material. Taking as a basis this observation, this paper shows that this coupling makes manifest at the signal level in the form of a set of properties only satisfied in uniform reflectance image areas. Such properties are deeply analyzed and formalized throughout this paper. It is also evidenced that their geometric interpretation allows enunciating a very-easy-to-check compatibility relationship between pixels about whether they share the same reflectance or not. Finally, an edge detector based on the use of the previous relationship is presented as an example of application. This edge detector inherits all the properties of the compatibility relationship: simplicity, low computational power requirements, sensor noise adaptivity and insensitivity to image intensity changes due to scene objects curvature.

Key words: Physics-based vision, Colour, Edge detection

* Corresponding author: Edificio Anselm Turmeda - Campus UIB, Cra. Valldemossa, km 7.5, 07071 Palma de Mallorca (SPAIN). Tel: +34 971 172992, Fax: +34 971 173003

Email addresses: alberto.ortiz@uib.es (Alberto Ortiz), goliver@uib.es (Gabriel Oliver).

URL: http://dmi.uib.es/~aortiz (Alberto Ortiz).

1. Introduction

Throughout the years, several methods have been proposed to locate uniform reflectance areas in images, being photometric invariants and the analysis of cluster structures in colour space the two most studied approaches (see [1–6], just to cite some of them). Image noise, however, deforms clusters and makes photometric invariants to be not so invariant, which makes the quality of the results conditional on the accuracy of the estimation of the clusters parameters or the invariant values. Several strategies have been reported in the related literature in order to counteract those undesired effects. For instance, Ohta et al. [7] and Healey [8] only consider, when computing photometric invariants, RGB values above a certain threshold, which is determined adaptively in the case of Healey. On the other hand, Klinker et al. [3] allow clusters of a certain thickness in accordance to sensor noise. Some others resort to more elaborated methods, such as the case of Gevers and Stokman [9], which make use of variable kernel density estimation and propagation of sensor noise to construct robust colour invariant histograms.

Overcoming those problems and providing a novel solution is the main motivation of this work. The new approach derives from the coupling which can be observed among colour channels in areas of uniform reflectance. In other words, in such areas, colour channels are not free to take any intensity value, but they depend on the values taken by the other colour channels. As will be seen along the following sections, this paper presents a formal and deep analysis of colour channel behaviour in those areas. Such analysis has derived in the formulation of a total of three properties which formalize several aspects of the coupling. Moreover, the coupling properties admit a geometrical interpretation through the plane of possible intensity values attainable by any combination of colour channels. As a result, a relation of compatibility $\mathcal{C}$ between pairs of pixels has been derived from the three properties, in the sense that if any of the three properties fails to be met by a certain couple of pixels for any combination of spectral (colour) channels, then it is impossible that both pixels belong to the same scene material. Therefore, all three properties become a sort of necessary conditions for searching areas of uniform reflectance in the image. In a noiseless environment, checking $\mathcal{C}$ is as simple as determining the orientation of a given vector in the aforementioned space. To cover noisy environments, $\mathcal{C}$ is redefined through the incorporation of intensity uncertainties derived from a noise model related with the operation of real imaging sensors, what does not increase complexity significantly. To finish, the limitations of the coupling analysis are also discussed. Summing up, the main contribution of this paper is the colour channel analysis here presented and ultimately the formal derivation of relation $\mathcal{C}$.

The analysis is based on the Dichromatic Reflection Model (DRM) [10], the most often referenced and used physics-based model of image formation, due to its general validity. Moreover, in order to widen the

applicability of the colour channel coupling analysis here presented, the usual expression for the DRM has been extended with a term accounting for ambient illumination, what is ignored by most physics-based vision algorithms. It is also noteworthy that the coupling analysis results to be independent of particular expressions of the different (spectral and non-spectral) terms of the DRM.

Although the applicability of the results of the previous analysis is obvious for *edge detection* and *image segmentation* tasks, they can also turn out to be useful whenever uniform reflectance areas of the image must be identified, such as, for instance, for *shape from shading* tasks. By way of illustration of the aforementioned, the paper finishes with the additional proposal of a novel edge detection technique based on $\mathcal{C}$ which inherits all its features: simplicity, low computational power requirements, sensor noise adaptivity and insensitivity to image intensity changes due to scene objects curvature. (See [11] for a segmentation algorithm founded on the same principles.)

The rest of the paper is organized as follows: first, section 2 revises the most relevant features of the DRM and presents with detail the model of image formation which has been assumed in this work; next, sections 3, 4, 5 and 6 investigate on the properties of uniform reflectance areas according to the image formation model presented in section 2; section 7 enunciates a compatibility relationship among pixels based on the colour channel coupling analysis proposed in the previous sections; section 8 discusses about the coverage of reflectance transitions achieved by analysis of colour channels coupling; section 9 relates colour channel coupling analysis with similar work; section 10 comments on the use of all the aforementioned to compute an edge map representing the reflectance changes of the imaged scene; finally, section 11 concludes the paper.

2. Physics-based Models of Image Formation

2.1. *Global overview*

Generally speaking, irradiance values measured at pixel locations are a combination of several scene factors which interact with each other: the illumination distribution, the reflection properties of scene objects –which in particular determine the colour (red, green, light blue, etc) by which we perceive them–, the objects geometry, both at the macroscopic and microscopic level (surface roughness), the propagation medium and the performance of the imaging sensor. The final pixel value is eventually determined by the (physical) laws that rule the processes of light propagation, reflection and image acquisition. Researchers using those models to develop vision algorithms have mostly focused their attention to the light-matter interaction part

of the image formation process. In this respect, a lot of knowledge has been gained throughout the years with contributions coming from fields such as radiant heat transfer, energy conservation, computer graphics and vision itself [12–14]. Of particular importance to the computer vision community are the developments of several models of reflection manageable enough so as to be effectively incorporated in machine vision algorithms at the cost of some loss of physical accuracy.

One of those models is the often-cited Dichromatic Reflection Model (DRM) proposed by Shafer [10]. The DRM was initially conceived for inhomogeneous dielectric (ID) materials, i.e. materials consisting of a medium comprising the bulk of the surface matter and suspended particles responsible of scattering and coloration effects. This class of materials include most paints, varnishes, paper, ceramics (including porcelain), plastics, etc. but does not comprise materials that are optically homogeneous, such as metals and many crystals. As shown in equation 1, the DRM expresses the radiance at a given scene point p for a certain wavelength λ as a sum of two reflection components: body (also referred to as diffuse) reflection, and interface (also referred to as specular) reflection.

$$L(p;\lambda) = \overbrace{m_b(p)\left[L_d(\lambda)\rho_b(p;\lambda)\right]}^{L_b(p;\lambda)} + \overbrace{m_i(p)\left[L_d(\lambda)\rho_i(p;\lambda)\right]}^{L_i(p;\lambda)} . \tag{1}$$

As can be seen, in the DRM, each reflection component L_j ($j \in \{b, i\}$) is modeled as the product of two terms: (1) $C_j(p;\lambda) = L_d(\lambda)\rho_j(p;\lambda)$, dependent only on wavelength and not on local geometry, and expressing the fraction of the incoming (directional) light $L_d(\lambda)$ which is conveyed by that reflection component due to the corresponding (body or interface) reflectance $0 \leq \rho_j(p;\lambda) \leq 1$; and (2) $m_j(p)$, which is a geometrical factor depending on the surface geometry at point p, and independent of wavelength. One important property of the DRM is this separability of the spectral and the non-spectral (geometric) factors. According to Shafer, the separation of the interface reflection component into a geometrical and a spectral term has an effect no greater than 2% in pixel-value errors, and this value is attained only if the angle of incidence of the light is larger than 60° and the viewing angle is nearly the perfect specular direction. As for the body reflection component, only if $L_d(p;\lambda)\rho_i(p;\lambda)$ is not constant there is an interdependence between the geometry and the spectral factors; since it generally does not vary much with wavelength, the effect of this interdependence is negligible.

The validity of the DRM for a large number of surface materials has been experimentally checked by several researchers:

– Tominaga and Wandell [15,16] tested the adequacy of the DRM for a number of inhomogeneous materials under the additional assumption of the constancy of the interface component of the reflectance $\rho_i(\lambda)$.

They reported to apply well for plastic, paint, ceramic, vinyl, fruit and leaves; however, it failed on metal, textiles and paper.

– Lee et al. [17] further investigated the constancy of $\rho_i(\lambda)$, providing essentially the same results as Tominaga and Wandell (i.e. adequacy for certain kinds of plastics, leaves, painted surfaces and fruits and inadequacy for other inhomogeneous materials such as coloured paper and some ceramics) and coined the term *Neutral Interface Reflection* model (NIR) for this particularization of the DRM.
– In a contemporary paper [18], Healey showed that: (a) using the Reichman body-scattering model [19], the DRM was a reasonable approximation for a large class of inhomogeneous dielectrics; and (b) from the Torrance-Sparrow surface-reflection model and the Fresnel equations, a simple model of the form

$$L(p;\lambda) = \overbrace{m_i(p)\left[L_d(\lambda)\rho_i(p;\lambda)\right]}^{L_i(p;\lambda)} \tag{2}$$

was an accurate color reflection model for metals under a single spectral composition of illumination. This model was called the *Unichromatic Reflection Model for metals* (URM). With both models, DRM and URM, Healey proposed the *Approximate Color Reflectance Model* (ACRM):

$$L(p;\lambda) = \begin{cases} m_i(p)C_i(p;\lambda) & \text{metal} \\ m_i(p)C_i(p;\lambda) + m_b(p)C_b(p;\lambda) & \text{ID} \end{cases} \tag{3}$$

– Later, Tominaga [20, 21] proposed a total of three variants of the basic DRM to describe the reflection properties of most materials: the Type I model is for inhomogeneous dielectric materials, such as plastics, and assumes that surface reflection consists of body reflection and interface reflection, being the latter independent of wavelength; the Type II model is for clothing and papers and allows wavelength-dependent interface reflection; finally, the Type III model is for metals and only incorporates interface reflection.
– Finally, Hashimoto et al. [22] applied the DRM to a single image to distinguish between metalic, matte non-metallic and glossy non-metallic surface types.

There are other models of image formation but they all can be assimilated to the general structure of the DRM or parts of it, since they mainly give more or less sophisticated, but separable, expressions for L_b and L_i. Briefly, Oren, Nayar and Wolff proposed in [23–25] more accurate models of body reflection, alternative to the usually employed Lambertian model, while detailed descriptions of interface reflection can also be found in the form of the Torrance-Sparrow [26], the Beckmann-Spizzichino [27] and the Cook-Torrance [28] models, or as simplifications of the former by Healey [18] and Healey and Binford [29]. Alternatively, the Phong model [30] provides simplicity and, despite not being founded on a sound physical basis, a surprisingly

remarkable realism. Similarly, Ward's model [31] was derived empirically from reflectance data obtained using an imaging gonioreflectometer, without a thorough consideration of the physics of light reflection. Finally, Tagare and de Figueiredo [32] present a model consisting of four reflection terms, the ideal specular lobe, the normal lobe, the forescatter lobe and the backscatter lobe, so that the DRM becomes a particular case covering the normal and forescatter lobes. While the ideal specular lobe is rarely encountered in practice, the backscatter lobe is most apparent from particulate surfaces such as sand or dry soil [33] (it has been observed in studies of the surface of the Moon and other planetary bodies).

Summing up, the DRM has proved to be adequate to most materials [34]. It is because of this general application that the study presented in this paper has focused on the DRM and its properties.

2.2. *Model of image formation assumed in this work*

The DRM as presented before depends on the assumption that the illumination at any point comes from a single light source. A further improvement over the model can be made by incorporating an ambient lighting term $L_a(p;\lambda) = L_a(\lambda)\rho_a(p;\lambda)$, representing light coming from all directions in equal amounts, $L_a(\lambda)$, which increases the radiance from scene surfaces independently of local surface geometry [10]. The reflectance term in this case, ρ_a, is generally expressed as a linear combination of the body and interface reflectances since the light reflected contains a part due to interface reflection and a part due to body reflection [10,35]. After adding the ambient term, the DRM turns out to be:

$$L(p;\lambda) = \overbrace{L_a(\lambda)\rho_a(p;\lambda)}^{L_a(p;\lambda)} + \overbrace{m_b(p)\left[L_d(\lambda)\rho_b(p;\lambda)\right]}^{L_b(p;\lambda)} + \overbrace{m_i(p)\left[L_d(\lambda)\rho_i(p;\lambda)\right]}^{L_i(p;\lambda)} . \tag{4}$$

As pointed out by Shafer [10], this model is a better approximation of daylight, that contains directional light from a point source (L_d terms), the sun, and ambient light from the sky (L_a term), and of light in a room, which comes from (directional) light fixtures (L_d terms) and from inter-reflections on walls and other objects (L_a term).

Finally, the pixel values provided by a camera are generally accepted as coming from [36]:

$$D^c(i,j) = q_0^c \int_\Lambda E(i,j;\lambda)\tau^c(\lambda)s(\lambda)d\lambda\,, \tag{5}$$

where: $D^c(i,j)$ is the digital value of the c colour channel at image cell (i,j); Λ represents the set of wavelengths in the visible spectrum (approximately between 380 (blue) and 760 (red) nanometers); q_0^c is a scaling factor which accounts for several elements influencing the whole image, such as the exposure time and the gain for the c colour channel; $E(i,j;\lambda)$ is the incoming light at image cell (i,j); $\tau^c(\lambda)$ is the filter

transmittance for the c colour channel, expressing the fraction of light that the corresponding colour filter allows reaching the image cell at each wavelength; and $s(\lambda)$ is the spectral responsivity of the sensor, which represents the degree of sensitiveness of the sensor to the different wavelengths. In a typical RGB camera, $c \in \{r, g, b\}$, while in a monochrome camera, $\tau(\lambda) = 1$. There exist other more complex models about camera operation (see, for instance, [37]), although the one commented above is enough in most vision tasks.

From a theoretical point of view, the relation between the radiance $L(p; \lambda)$ at the scene points p optically reachable from the collection site (i, j) under consideration and the corresponding irradiance $E(i, j; \lambda)$ involves the interaction with the propagation medium together with the effects of the camera optics on the arriving light through its *point-spread function* and the *lens collection* capability. Assuming a non-attenuating propagation medium and ignoring the blurring and low-pass filtering effects of the point-spread function of the optics in a properly focused camera, the relation between irradiance at the collection site E and scene radiance L was shown to be [38]:

$$E = \frac{\pi}{4} \left(\frac{d}{f} \right)^2 \cos^4 \phi \, L \,, \tag{6}$$

where d is the effective diameter of the lens according to the optics aperture, f is the focal distance and ϕ is the angle between the ray from the scene point to the center of projection and the optical axis.

Combining equations 4, 5 and 6, a compact and useful expression for the model of image formation can be obtained:

$$D^c(i, j) = C_a^c(i, j) + m_b(i, j) C_b^c(i, j) + m_i(i, j) C_i^c(i, j) \,, \tag{7}$$

where C_a^c, C_b^c and C_i^c are, respectively, the so-called *ambient*, *body* and *interface composite reflectances*, representing the joint contribution of lighting and material reflectance to the corresponding reflection component.

3. General Properties of Uniformly Coloured Image Areas

Within an image area whose pixels correspond to scene points belonging to the same material, the ambient, body and interface colours are constant (i.e. $\rho_b(i, j; \lambda) = \rho_b(\lambda)$ and $\rho_i(i, j; \lambda) = \rho_i(\lambda)$ and, by extension, also $\rho_a(i, j; \lambda) = \rho_a(\lambda)$ because of its dependence on exclusively ρ_b and ρ_i). In a noiseless environment, changes in the pixel values between image locations are, thus, only due to changes in the geometrical factors m_b and m_i. As a consequence, in areas of uniform reflectance, colour channels keep coupled, in the sense that they are not free to take any intensity value, but they depend on the values taken by the other colour channels through the body and interface reflectances and the way they are combined in the image formation model.

As a result of the study of this coupling, up to three necessary compatibility conditions have been identified. They are formulated in the form of the following properties:

Property 1 *For any pair of colour channels c_1 and c_2 and any two image locations $p_1 = (i_1, j_1)$ and $p_2 = (i_2, j_2)$ corresponding to the same scene material,*

$$(1)\ D^{c_1}(p_1) \geq D^{c_2}(p_1) \Leftrightarrow D^{c_1}(p_2) \geq D^{c_2}(p_2)\,, \quad (2)\ D^{c_1}(p_1) \leq D^{c_2}(p_1) \Leftrightarrow D^{c_1}(p_2) \leq D^{c_2}(p_2)$$

Property 2 *For any pair of colour channels c_1 and c_2, any image location $p = (i, j)$ not corresponding to a material change, and any direction ξ over the image plane,*

$$(1)\ \left(\frac{dD^{c_1}(p)}{d\xi}\right) \geq 0 \Leftrightarrow \left(\frac{dD^{c_2}(p)}{d\xi}\right) \geq 0\,, \quad (2)\ \left(\frac{dD^{c_1}(p)}{d\xi}\right) \leq 0 \Leftrightarrow \left(\frac{dD^{c_2}(p)}{d\xi}\right) \leq 0$$

Property 3 *For any pair of colour channels c_1 and c_2 and any two image locations $p_1 = (i_1, j_1)$ and $p_2 = (i_2, j_2)$ corresponding to the same scene material,*

$$\left.\begin{array}{l}(1.1)\ D^{c_1}(p_1) \geq D^{c_1}(p_2) \text{ and } D^{c_1}(p_1) \geq D^{c_2}(p_1), \text{ or} \\ (1.2)\ D^{c_1}(p_1) \leq D^{c_1}(p_2) \text{ and } D^{c_1}(p_1) \leq D^{c_2}(p_1)\end{array}\right\} \Leftrightarrow D^{c_1}(p_1) - D^{c_2}(p_1) \geq D^{c_1}(p_2) - D^{c_2}(p_2)$$

$$\left.\begin{array}{l}(2.1)\ D^{c_1}(p_1) \geq D^{c_1}(p_2) \text{ and } D^{c_1}(p_1) \leq D^{c_2}(p_1), \text{ or} \\ (2.2)\ D^{c_1}(p_1) \leq D^{c_1}(p_2) \text{ and } D^{c_1}(p_1) \geq D^{c_2}(p_1)\end{array}\right\} \Leftrightarrow D^{c_1}(p_1) - D^{c_2}(p_1) \leq D^{c_1}(p_2) - D^{c_2}(p_2)$$

The previous properties characterize in fact the three following behaviours:

- *Colour channels do not cross one another* (property 1). As a consequence, colour channels are *ordered* in regions of uniform reflectance in the sense that, if for pixel $p_1 = (i_1, j_1)$ the intensity for channel c_1 is "above" the intensity of channel c_2 (i.e. the intensity in channel c_1 is larger than in channel c_2), then for any pixel $p_2 = (i_2, j_2)$ in the same region, colour channel c_1 will also be "above" colour channel c_2.

- *Colour channels vary in a coordinated way: when one changes, so do the others, and in the same sense, all increase or all decrease* (property 2). Observe that another form of this property is as follows: "*Given two image locations $p_1 = (i_1, j_1)$ and $p_2 = (i_2, j_2)$ corresponding to the same scene material, $D^{c_1}(p_1) \geq D^{c_1}(p_2)$ if and only if $D^{c_2}(p_1) \geq D^{c_2}(p_2)$, and the same applies for $\leq$*".

- *As the intensity in one channel decreases, so does the difference between colour channel intensities; the opposite happens when the intensity in one channel increases* (property 3). Notice that the property is formulated so as to take into account the four possible cases:

  (a) $D^{c_1}(p_1) \geq D^{c_2}(p_1)$ (channel c_1 is "above" channel c_2) and

  (i) $D^{c_1}(p_1) \geq D^{c_1}(p_2)$ (intensity decreases between p_1 and p_2),

  $D^{c_1}(p_1) - D^{c_2}(p_1) \geq 0$ is above $D^{c_1}(p_2) - D^{c_2}(p_2) \geq 0$ [case (1.1)]

  (ii) $D^{c_1}(p_1) \leq D^{c_1}(p_2)$ (intensity increases between p_1 and p_2),

  $D^{c_1}(p_1) - D^{c_2}(p_1) \geq 0$ is below $D^{c_1}(p_2) - D^{c_2}(p_2) \geq 0$ [case (2.2)]

  (b) $D^{c_1}(p_1) \leq D^{c_2}(p_1)$ (channel c_1 is "below" channel c_2) and

  (i) $D^{c_1}(p_1) \geq D^{c_1}(p_2)$ (intensity decreases between p_1 and p_2),

  $D^{c_1}(p_1) - D^{c_2}(p_1) \leq 0$ is below $D^{c_1}(p_2) - D^{c_2}(p_2) \leq 0$ [case (2.1)]

  (ii) $D^{c_1}(p_1) \leq D^{c_1}(p_2)$ (intensity increases between p_1 and p_2),

  $D^{c_1}(p_1) - D^{c_2}(p_1) \leq 0$ is above $D^{c_1}(p_2) - D^{c_2}(p_2) \leq 0$ [case (1.2)]

4. Particularization of the General Properties

The fulfillment of properties 1-3 depends on the particular instantiation of the image formation model (equation 7). Four cases are distinguished:

- *Case 1: non-glossy pixels/without ambient lighting*
- *Case 2: non-glossy pixels/with ambient lighting*
- *Case 3: glossy pixels/without ambient lighting*
- *Case 4: glossy pixels/with ambient lighting*

They are all revised in the following sections.

4.1. *Case 1: non-glossy pixels/without ambient lighting*

If interface reflection and ambient lighting are not taken into account, the intensity of every colour channel is reduced to the following expression:

$$D^c(i,j) = m_b(i,j)C_b^c(i,j)\,. \tag{8}$$

In such a case, the three properties are met. In other words, assuming the model of equation 8, in uniform reflectance areas, colour channels do not cross one another, they vary coordinately, and the difference

between colour channel intensities decreases as the intensity in anyone of them decreases. These facts are stated in the following three propositions, whose proofs can be found in [11, Appendix B].

Proposition 1 *Assuming ambient lighting is negligible and directional illumination is uniform throughout the scene, for any pair of colour channels c_1 and c_2, and any two image locations $p_1 = (i_1, j_1)$ and $p_2 = (i_2, j_2)$ coming from the same scene material, such that interface reflection is negligible, i.e. $D_i^c(p_1) = 0$ and $D_i^c(p_2) = 0$,*

$$(1)\ D^{c_1}(p_1) \geq D^{c_2}(p_1) \Leftrightarrow D^{c_1}(p_2) \geq D^{c_2}(p_2)\,, \quad (2)\ D^{c_1}(p_1) \leq D^{c_2}(p_1) \Leftrightarrow D^{c_1}(p_2) \leq D^{c_2}(p_2)$$

Proposition 2 *Assuming ambient lighting is negligible and directional illumination is uniform throughout the scene, for any pair of colour channels c_1 and c_2, any image location $p = (i, j)$ not corresponding to a material change, such that interface reflection is negligible, i.e. $D_i^c(p) = 0$, and any direction ξ over the image plane,*

$$(1)\ \left(\frac{dD^{c_1}(p)}{d\xi}\right) \geq 0 \Leftrightarrow \left(\frac{dD^{c_2}(p)}{d\xi}\right) \geq 0\,, \quad (2)\ \left(\frac{dD^{c_1}(p)}{d\xi}\right) \leq 0 \Leftrightarrow \left(\frac{dD^{c_2}(p)}{d\xi}\right) \leq 0$$

Proposition 3 *Assuming ambient lighting is negligible and directional illumination is uniform throughout the scene, for any pair of colour channels c_1 and c_2, and any two image locations $p_1 = (i_1, j_1)$ and $p_2 = (i_2, j_2)$ coming from the same scene material, such that interface reflection is negligible, i.e. $D_i^c(p_1) = 0$ and $D_i^c(p_2) = 0$,*

$$\left.\begin{array}{l}(1.1)\ D^{c_1}(p_1) \geq D^{c_1}(p_2) \text{ and } D^{c_1}(p_1) \geq D^{c_2}(p_1), \text{ or} \\ (1.2)\ D^{c_1}(p_1) \leq D^{c_1}(p_2) \text{ and } D^{c_1}(p_1) \leq D^{c_2}(p_1)\end{array}\right\} \Leftrightarrow D^{c_1}(p_1) - D^{c_2}(p_1) \geq D^{c_1}(p_2) - D^{c_2}(p_2)$$

$$\left.\begin{array}{l}(2.1)\ D^{c_1}(p_1) \geq D^{c_1}(p_2) \text{ and } D^{c_1}(p_1) \leq D^{c_2}(p_1), \text{ or} \\ (2.2)\ D^{c_1}(p_1) \leq D^{c_1}(p_2) \text{ and } D^{c_1}(p_1) \geq D^{c_2}(p_1)\end{array}\right\} \Leftrightarrow D^{c_1}(p_1) - D^{c_2}(p_1) \leq D^{c_1}(p_2) - D^{c_2}(p_2)$$

4.2. *Case 2: non-glossy pixels/with ambient lighting*

Now, the resultant image formation model is given by:

$$D^c(i, j) = C_a^c(i, j) + m_b(i, j) C_b^c(i, j)\,. \tag{9}$$

In this case, only property 2 is met in general. Properties 1 and 3 require an additional hypothesis to be applicable. All these facts are stated in the following lemma and propositions: (As before, formal proofs can be found in [11, Appendix B].)

Lemma 1 *If ambient illumination is proportional to directional illumination (i.e.* $L_a(\lambda) = \alpha L_d(\lambda)$ $[\alpha \geq 0], \forall\lambda$*) and interface reflection is not involved in the reflected light, then, for any material and any two colour channels* c_1 *and* c_2*:*

$$(1)\ C_a^{c_1} \geq C_a^{c_2} \Leftrightarrow C_b^{c_1} \geq C_b^{c_2}\,, \quad (2)\ C_a^{c_1} \leq C_a^{c_2} \Leftrightarrow C_b^{c_1} \leq C_b^{c_2}$$

Proposition 4 *Assuming directional illumination is uniform throughout the scene and ambient illumination is proportional to directional illumination, for any pair of colour channels* c_1 *and* c_2*, and any two image locations* $p_1 = (i_1, j_1)$ *and* $p_2 = (i_2, j_2)$ *coming from the same scene material, such that interface reflection is negligible, i.e.* $D_i^c(p_1) = 0$ *and* $D_i^c(p_2) = 0$*,*

$$(1)\ D^{c_1}(p_1) \geq D^{c_2}(p_1) \Leftrightarrow D^{c_1}(p_2) \geq D^{c_2}(p_2)\,, \quad (2)\ D^{c_1}(p_1) \leq D^{c_2}(p_1) \Leftrightarrow D^{c_1}(p_2) \leq D^{c_2}(p_2)$$

Proposition 5 *Assuming directional illumination is uniform throughout the scene, for any pair of colour channels* c_1 *and* c_2*, any image location* $p = (i, j)$ *not corresponding to a material change, such that interface reflection is negligible, i.e.* $D_i^c(p) = 0$*, and any direction* ξ *over the image plane,*

$$(1)\ \left(\frac{dD^{c_1}(p)}{d\xi}\right) \geq 0 \Leftrightarrow \left(\frac{dD^{c_2}(p)}{d\xi}\right) \geq 0\,, \quad (2)\ \left(\frac{dD^{c_1}(p)}{d\xi}\right) \leq 0 \Leftrightarrow \left(\frac{dD^{c_2}(p)}{d\xi}\right) \leq 0$$

Proposition 6 *Assuming directional illumination is uniform throughout the scene and ambient illumination is proportional to directional illumination, for any pair of colour channels* c_1 *and* c_2*, and any two image locations* $p_1 = (i_1, j_1)$ *and* $p_2 = (i_2, j_2)$ *coming from the same scene material, such that interface reflection is negligible, i.e.* $D_i^c(p_1) = 0$ *and* $D_i^c(p_2) = 0$*,*

$$\left.\begin{array}{l}(1.1)\ D^{c_1}(p_1) \geq D^{c_1}(p_2) \text{ and } D^{c_1}(p_1) \geq D^{c_2}(p_1), \text{ or} \\ (1.2)\ D^{c_1}(p_1) \leq D^{c_1}(p_2) \text{ and } D^{c_1}(p_1) \leq D^{c_2}(p_1)\end{array}\right\} \Leftrightarrow D^{c_1}(p_1) - D^{c_2}(p_1) \geq D^{c_1}(p_2) - D^{c_2}(p_2)$$

$$\left.\begin{array}{l}(2.1)\ D^{c_1}(p_1) \geq D^{c_1}(p_2) \text{ and } D^{c_1}(p_1) \leq D^{c_2}(p_1), \text{ or} \\ (2.2)\ D^{c_1}(p_1) \leq D^{c_1}(p_2) \text{ and } D^{c_1}(p_1) \geq D^{c_2}(p_1)\end{array}\right\} \Leftrightarrow D^{c_1}(p_1) - D^{c_2}(p_1) \leq D^{c_1}(p_2) - D^{c_2}(p_2)$$

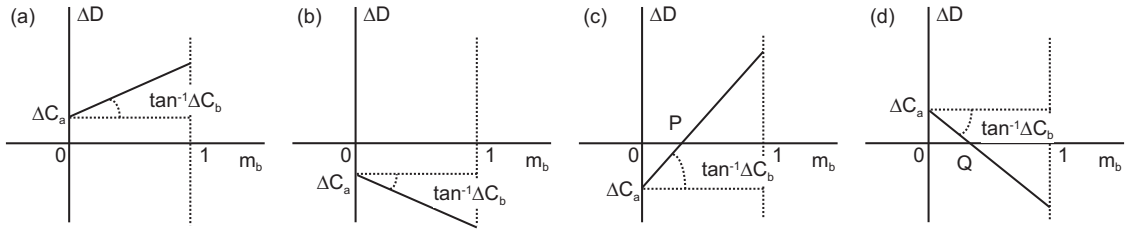

Fig. 1. Four possible configurations of the straight line $\Delta D(p) = \Delta C_a + m_b(p)\Delta C_b$ $(p = (i, j))$.

Observe that the new formulation for properties 1 and 3 comes from the introduction of the ambient reflection term, which has led to the fact that the sign of $D^{c_1}(p) - D^{c_2}(p)$ does not determine, in the general case, the sign of the difference for any other image point for the same scene material. In effect, for all the points $p = (i, j)$ belonging to the same scene material, the differences between colour channels c_1 and c_2, $\Delta D(p) = D^{c_1}(p) - D^{c_2}(p) = (C_a^{c_1} - C_a^{c_2}) + m_b(p)(C_b^{c_1} - C_b^{c_2}) = \Delta C_a + m_b(p)\Delta C_b$, lie in a straight line with variables ΔD and m_b and parameters ΔC_a (intercept with ΔD axis) and ΔC_b (slope with m_b axis). This straight line can adopt any of the four configurations shown in figure 1. In cases (a) and (b), the signs of ΔC_a and ΔC_b are the same and, thus, coincide with the sign of ΔD for any value of m_b. However, in cases (c) and (d), the signs of ΔC_a and ΔC_b are different and only if $m_b(p_1)$ and $m_b(p_2)$ are both above or both below $P = Q = -\frac{\Delta C_a}{\Delta C_b}$ the signs of the differences $D^{c_1}(p_1) - D^{c_2}(p_1)$ and $D^{c_1}(p_2) - D^{c_2}(p_2)$ are the same. The constraint relating ambient lighting with directional illumination through the scale factor $\alpha \geq 0$ in propositions 4 and 6 force situations (a) and (b) everywhere in the scene.

4.3. *Case 3: glossy pixels/without ambient lighting*

In this case, the intensity of every colour channel is given by the following expression:

$$D^c(i, j) = m_b(i, j)C_b^c(i, j) + m_i(i, j)C_i^c(i, j)\,. \tag{10}$$

When interface reflection is introduced in the formation model, only property 1 is satisfied after a slight modification of the formulation, as it is indicated in the following proposition: (For the formal proof see again [11, Appendix B].)

Proposition 7 *Assuming ambient lighting is negligible and directional illumination is uniform throughout the scene, and assuming the NIR formation model, for any pair of colour channels c_1 and c_2, and any two image locations $p_1 = (i_1, j_1)$ and $p_2 = (i_2, j_2)$ coming from the same scene material,*

$$(1)\ D^{c_1}(p_1) \geq D^{c_2}(p_1)\frac{L_d^{c_1}}{L_d^{c_2}} \Leftrightarrow D^{c_1}(p_2) \geq D^{c_2}(p_2)\frac{L_d^{c_1}}{L_d^{c_2}}\,, \quad (2)\ D^{c_1}(p_1) \leq D^{c_2}(p_1)\frac{L_d^{c_1}}{L_d^{c_2}} \Leftrightarrow D^{c_1}(p_2) \leq D^{c_2}(p_2)\frac{L_d^{c_1}}{L_d^{c_2}}$$

where $L_d^c = q_0^c \int_\Lambda L_d(\lambda)\tau^c(\lambda)s(\lambda)d\lambda$ *is the (scaled) radiance of the directional light source for channel* c.

In order for the previous proposition to be applicable, L_d^c must thus be estimated for every colour channel c for the particular scene. Any of the methods presented in [11, Chapter 5] or in any other publication regarding the estimation of the lighting parameters can be used for this purpose.

As for property 2, it is no longer true in general when interface reflection is incorporated into the reflection model. This is because the derivative of the intensity in every channel not only depends now on the sign of the derivative of m_b but also on the derivative of m_i (note that C_b and C_i are constant in a uniform reflectance area). For $p = (i, j)$:

$$\left(\frac{dD^{c_1}(p)}{d\xi}\right) = m_b'(p)C_b^{c_1} + m_i'(p)C_i^{c_1}\,, \quad \left(\frac{dD^{c_2}(p)}{d\xi}\right) = m_b'(p)C_b^{c_2} + m_i'(p)C_i^{c_2},$$

where $m_b'(p)$ and $m_i'(p)$ are the first-order derivatives along direction ξ of $m_b(p)$ and $m_i(p)$, respectively. As a consequence, in general:

$$m_b'(p)C_b^{c_1} + m_i'(p)C_i^{c_1} \lesseqgtr 0 \quad m_b'(p)C_b^{c_2} + m_i'(p)C_i^{c_2} \lesseqgtr 0$$

$$\Updownarrow \qquad\qquad \Updownarrow$$

$$m_b'(p)C_b^{c_1} \lesseqgtr -m_i'(p)C_i^{c_1} \not\Leftrightarrow m_b'(p)C_b^{c_2} \lesseqgtr -m_i'(p)C_i^{c_2}$$

Observe that the derivatives of both channels c_1 and c_2 will have the same sign if m_b' and m_i' are both positive or both negative, or, in case their signs do not coincide, if the derivative of the same reflection component dominates the sum in both cases (i.e. $|m_b'(p)C_b^{c_1}| \lesseqgtr |m_i'(p)C_i^{c_1}|$ and $|m_b'(p)C_b^{c_2}| \lesseqgtr |m_i'(p)C_i^{c_2}|$). By way of example, in the intensity profiles of figure 2, the dotted lines enclose an area where m_b' and m_i' have different sign, but the derivatives of every colour channel have all the same sign.

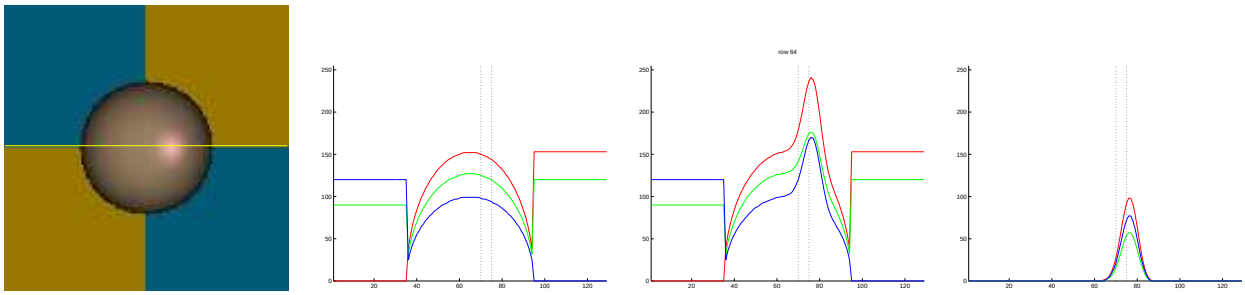

(a) (b) (c) (d)

Fig. 2. (a) A synthetic image without ambient lighting, (b) intensity profile for row 64 (in yellow) for every colour channel, (c) body component profiles, and (d) interface component profiles.

Finally, as for property 3, figure 2 shows precisely a case where it is not met. In effect, the intensity levels of the green and blue channels within the area enclosed by the dotted lines are such that, when the intensity increases in both, the difference between both channels does not increase, but decreases.

4.4. *Case 4: glossy pixels/with ambient lighting*

In the general case:

$$D^c(i,j) = C_a^c(i,j) + m_b(i,j)C_b^c(i,j) + m_i(i,j)C_i^c(i,j)\,. \tag{11}$$

With the incorporation of the interface reflection term, only property 1 holds after the changes in the formulation already introduced in case 3. The NIR model is again assumed, together with an ambient illumination proportional to the directional lighting. The following lemma and proposition states the aforementioned in a formal way: (See [11, Appendix B] for the formal proofs as before.)

Lemma 2 *If ambient illumination is proportional to directional illumination (i.e.* $L_a(\lambda) = \alpha L_d(\lambda)$ $[\alpha \geq 0], \forall\lambda$*) and if the NIR formation model is assumed, for any material and any two colour channels* c_1 *and* c_2*:*

$$(1)\ C_a^{c_1} - C_a^{c_2}\frac{L_d^{c_1}}{L_d^{c_2}} \geq 0 \Leftrightarrow C_b^{c_1} - C_b^{c_2}\frac{L_d^{c_1}}{L_d^{c_2}} \geq 0\,, \quad (2)\ C_a^{c_1} - C_a^{c_2}\frac{L_d^{c_1}}{L_d^{c_2}} \leq 0 \Leftrightarrow C_b^{c_1} - C_b^{c_2}\frac{L_d^{c_1}}{L_d^{c_2}} \leq 0$$

where $L_d^c = q_0^c \int_\Lambda L_d(\lambda)\tau^c(\lambda)s(\lambda)d\lambda$ *is the (scaled) radiance of directional illumination for colour channel* c*.*

Proposition 8 *Assuming directional illumination is uniform throughout the scene and that ambient illumination is proportional to directional illumination, and assuming the NIR formation model, for any pair of colour channels* c_1 *and* c_2*, and any two image locations* $p_1 = (i_1, j_1)$ *and* $p_2 = (i_2, j_2)$ *coming from the same scene material,*

$$(1)\ D^{c_1}(p_1) \geq D^{c_2}(p_1)\frac{L_d^{c_1}}{L_d^{c_2}} \Leftrightarrow D^{c_1}(p_2) \geq D^{c_2}(p_2)\frac{L_d^{c_1}}{L_d^{c_2}}\,, \quad (2)\ D^{c_1}(p_1) \leq D^{c_2}(p_1)\frac{L_d^{c_1}}{L_d^{c_2}} \Leftrightarrow D^{c_1}(p_2) \leq D^{c_2}(p_2)\frac{L_d^{c_1}}{L_d^{c_2}}$$

where $L_d^c = q_0^c \int_\Lambda L_d(\lambda)\tau^c(\lambda)s(\lambda)d\lambda$ *is the (scaled) radiance of directional illumination for channel* c*.*

As for properties 2 and 3, the same remarks as for case 3 apply here.

5. Summary on the Applicability of the Properties

By way of recapitulation of section 4, table 1 summarizes the dependence of the fulfillment of properties 1-3 on the particular instantiation of the image formation model. Some conclusions about the applicability of those properties can be drawn now that the four cases have been revised:

- When the interface reflection term is introduced, only property 1 is satisfied in general within uniform

Table 1
Fulfillment of properties 1-3 depending on the particular instantiation of the image formation model.

case	properties fulfilled and conditions
(1) matte pixels, no ambient lighting	properties 1-3 always
(2) matte pixels, ambient lighting	property 2 always; properties 1 and 3 if $L_a(\lambda) = \alpha L_d(\lambda), \alpha > 0$
(3) glossy pixels, no ambient lighting	property 1 under the NIR model and white-balanced images
(4) glossy pixels, ambient lighting	property 1 under the NIR model, white-balanced images and $L_a(\lambda) = \alpha L_d(\lambda), \alpha > 0$

reflectance areas. This means that false material changes can be detected sometimes inside or near specularities. As has been discussed before, it depends on whether the sign of m'_b or m'_i are the same or not, and on which term dominates the value of the derivative: the body/ambient reflection terms or the interface reflection term. Therefore, not always will specularities give rise to false material changes.

- Properties 1 and 3 require that L_a is proportional to L_d in order for them to be applicable when ambient lighting is not negligible. As was said in section 2, the ambient lighting comes, in an outdoor environment, from the sky through scattering in the atmosphere, or, in a room, from inter-reflections on the walls and other objects. Given these facts, it is obvious that some relationship can be expected between ambient lighting and directional lighting. Unfortunately, no physical evidence about the proportionality relationship has been found in the related literature, apart from other authors also making use of it, be directly [39] or indirectly by assuming white illumination [1, 40]. However, the experiments performed have shown that, in general, violations of properties 1 and 3 are closely related with reflectance transitions.

6. Cases which Fail to Satisfy the Properties

The following propositions characterize which are the circumstances under which properties 1-3 are not fulfilled: (As before, formal proofs are given in [11, Appendix B].)

Proposition 9 *Assuming directional illumination is uniform throughout the scene and that ambient illumination is proportional to directional illumination, and assuming the NIR formation model, for any pair of colour channels c_1 and c_2 and any two image locations $p_1 = (i_1, j_1)$ and $p_2 = (i_2, j_2)$:*

(1) $D^{c_1}(p_1) > D^{c_2}(p_1)\frac{L_d^{c_1}}{L_d^{c_2}}$ and $D^{c_1}(p_2) < D^{c_2}(p_2)\frac{L_d^{c_1}}{L_d^{c_2}} \Leftrightarrow C_b^{c_1}(p_1) > C_b^{c_2}(p_1)\frac{L_d^{c_1}}{L_d^{c_2}}$ and $C_b^{c_1}(p_2) < C_b^{c_2}(p_2)\frac{L_d^{c_1}}{L_d^{c_2}}$

(2) $D^{c_1}(p_1) < D^{c_2}(p_1)\frac{L_d^{c_1}}{L_d^{c_2}}$ and $D^{c_1}(p_2) > D^{c_2}(p_2)\frac{L_d^{c_1}}{L_d^{c_2}} \Leftrightarrow C_b^{c_1}(p_1) < C_b^{c_2}(p_1)\frac{L_d^{c_1}}{L_d^{c_2}}$ and $C_b^{c_1}(p_2) > C_b^{c_2}(p_2)\frac{L_d^{c_1}}{L_d^{c_2}}$

where $L_d^c = q_0^c \int_\Lambda L_d(\lambda)\tau^c(\lambda)s(\lambda)d\lambda$ *is the (scaled) radiance coming from the directional light source for channel c.*

Proposition 10 *Assuming directional illumination is uniform throughout the scene and that ambient illumination is proportional to directional illumination, for any pair of colour channels* c_1 *and* c_2 *and any two image locations* $p_1 = (i_1, j_1)$ *and* $p_2 = (i_2, j_2)$ *such that* $D_i^c(p_1) = 0$ *and* $D_i^c(p_2) = 0$,

$$(1)\ D^{c_1}(p_1) - D^{c_1}(p_2) > 0 \text{ and } D^{c_2}(p_1) - D^{c_2}(p_2) < 0 \Rightarrow \frac{C_b^{c_2}(p_1)}{C_b^{c_1}(p_1)} < \frac{C_b^{c_2}(p_2)}{C_b^{c_1}(p_2)}$$

$$(2)\ D^{c_1}(p_1) - D^{c_1}(p_2) < 0 \text{ and } D^{c_2}(p_1) - D^{c_2}(p_2) > 0 \Rightarrow \frac{C_b^{c_2}(p_1)}{C_b^{c_1}(p_1)} > \frac{C_b^{c_2}(p_2)}{C_b^{c_1}(p_2)}$$

Proposition 11 *Assuming directional illumination is uniform throughout the scene and that ambient illumination is proportional to directional illumination, for any pair of colour channels* c_1 *and* c_2 *and any two image locations* $p_1 = (i_1, j_1)$ *and* $p_2 = (i_2, j_2)$ *such that* $D_i^c(p_1) = 0$ *and* $D_i^c(p_2) = 0$,

$$(1)\ \left.\begin{array}{l} D^{c_1}(p_1) \geq D^{c_1}(p_2) \text{ and } D^{c_2}(p_1) \geq D^{c_2}(p_2) \\ D^{c_1}(p_1) \geq D^{c_2}(p_1) \text{ and } D^{c_1}(p_2) \geq D^{c_2}(p_2) \\ D^{c_1}(p_1) - D^{c_2}(p_1) < D^{c_1}(p_2) - D^{c_2}(p_2) \end{array}\right\} \Rightarrow \left\{\begin{array}{l} C_b^{c_1}(p_1) > C_b^{c_1}(p_2) \\ C_b^{c_2}(p_1) > C_b^{c_2}(p_2) \end{array}\right.$$

$$(2)\ \left.\begin{array}{l} D^{c_1}(p_1) \leq D^{c_1}(p_2) \text{ and } D^{c_2}(p_1) \leq D^{c_2}(p_2) \\ D^{c_1}(p_1) \leq D^{c_2}(p_1) \text{ and } D^{c_1}(p_2) \leq D^{c_2}(p_2) \\ D^{c_1}(p_1) - D^{c_2}(p_1) < D^{c_1}(p_2) - D^{c_2}(p_2) \end{array}\right\} \Rightarrow \left\{\begin{array}{l} C_b^{c_1}(p_1) < C_b^{c_1}(p_2) \\ C_b^{c_2}(p_1) < C_b^{c_2}(p_2) \end{array}\right.$$

$$(3)\ \left.\begin{array}{l} D^{c_1}(p_1) \geq D^{c_1}(p_2) \text{ and } D^{c_2}(p_1) \geq D^{c_2}(p_2) \\ D^{c_1}(p_1) \leq D^{c_2}(p_1) \text{ and } D^{c_1}(p_2) \leq D^{c_2}(p_2) \\ D^{c_1}(p_1) - D^{c_2}(p_1) > D^{c_1}(p_2) - D^{c_2}(p_2) \end{array}\right\} \Rightarrow \left\{\begin{array}{l} C_b^{c_1}(p_1) > C_b^{c_1}(p_2) \\ C_b^{c_2}(p_1) > C_b^{c_2}(p_2) \end{array}\right.$$

$$(4)\ \left.\begin{array}{l} D^{c_1}(p_1) \leq D^{c_1}(p_2) \text{ and } D^{c_2}(p_1) \leq D^{c_2}(p_2) \\ D^{c_1}(p_1) \geq D^{c_2}(p_1) \text{ and } D^{c_1}(p_2) \geq D^{c_2}(p_2) \\ D^{c_1}(p_1) - D^{c_2}(p_1) > D^{c_1}(p_2) - D^{c_2}(p_2) \end{array}\right\} \Rightarrow \left\{\begin{array}{l} C_b^{c_1}(p_1) < C_b^{c_1}(p_2) \\ C_b^{c_2}(p_1) < C_b^{c_2}(p_2) \end{array}\right.$$

Table 2
Reflectance transitions expressed by propositions 9-11 [$p_1 = (i_1, j_1), p_2 = (i_2, j_2)$].

proposition		**reflectance transition**		
9	CHannel Crossing (CHC)	$\rho_b^{c_1}(p_1) > \rho_b^{c_2}(p_1)$ $\rho_b^{c_1}(p_2) < \rho_b^{c_2}(p_2)$	or	$\rho_b^{c_1}(p_1) < \rho_b^{c_2}(p_1)$ $\rho_b^{c_1}(p_2) > \rho_b^{c_2}(p_2)$
10	Non-Coinciding Derivative (NCD)	$\frac{\rho_b^{c_2}(p_1)}{\rho_b^{c_1}(p_1)} < \frac{\rho_b^{c_2}(p_2)}{\rho_b^{c_1}(p_2)}$	or	$\frac{\rho_b^{c_2}(p_1)}{\rho_b^{c_1}(p_1)} > \frac{\rho_b^{c_2}(p_2)}{\rho_b^{c_1}(p_2)}$
11	Non-Decreasing Difference (NDD)	$\rho_b^{c_1}(p_1) > \rho_b^{c_1}(p_2)$ $\rho_b^{c_2}(p_1) > \rho_b^{c_2}(p_2)$	or	$\rho_b^{c_1}(p_1) < \rho_b^{c_1}(p_2)$ $\rho_b^{c_2}(p_1) < \rho_b^{c_2}(p_2)$

These last propositions deserve several observations:

- First of all, notice that every proposition identifies situations for which the composite body reflectances corresponding to image locations $p_1 = (i_1, j_1)$ and $p_2 = (i_2, j_2)$ must necessarily be different due to failure to fulfill one of properties 1-3. Although the reflectance changes are depicted by means of the respective composite body reflectances $C_b^{c_1}$ and $C_b^{c_2}$, they can also be expressed in terms of ρ_b as follows. Through the mean value theorem, the composite body reflectance for a certain colour channel c can be put as a product of two terms:

$$C_b^c(i,j) = q_0^c \int_\Lambda L_d(\lambda)\rho_b(i,j;\lambda)\tau^c(\lambda)s(\lambda)\ d\lambda = \rho_b(i,j;\lambda_0)\left[q_0^c \int_\Lambda L_d(\lambda)\tau^c(\lambda)s(\lambda)d\lambda\right],$$

  for some $\lambda_0 \in \Lambda$. Therefore, if $\rho_b^c(i,j) = \rho_b(i,j;\lambda_0)$ is defined for every colour channel and image location [1], then the three propositions correspond to the reflectance transitions enumerated in table 2. (The relationships between ρ_b^c's which are given are immediate from the proofs of the corresponding propositions.)

- Regarding proposition 9, cases (1) and (2) of its enunciate provide the only two ways to fail to fulfill property 1: the order between two colour channels intensity is reversed from location $p_1 = (i_1, j_1)$ to location $p_2 = (i_2, j_2)$. If those location happen to be adjacent to one another, then a reflectance transition of the type indicated in table 2 necessarily exists between p_1 and p_2, which materializes as

[1] Observe that $\rho_b^c(i,j) = \rho_b(i,j;\lambda_0)$ is the same for every (i,j) corresponding to the same scene material, provided that the illumination is uniform throughout the scene. Therefore, it is in fact a property of the material, although just for that particular scene. In effect, contrary to what can seem at first sight, $\rho_b^c(i,j)$ is not really illumination-independent since, in fact:

$$\rho_b^c(i,j) = \frac{\int_\Lambda L_d(\lambda)\rho_b(i,j;\lambda)\tau^c(\lambda)s(\lambda)\ d\lambda}{\int_\Lambda L_d(\lambda)\tau^c(\lambda)s(\lambda)d\lambda} \tag{12}$$

a colour channel crossing in-between both image locations.

Besides, observe that the proposition is written as a double implication. In order to illustrate this fact, let us consider, by way of example, case (1) of the proposition. In this case, channel c_1 is "above" channel c_2 at p_1 (i.e. the intensity in channel c_1 is larger than the intensity in channel c_2), while at p_2 is just the opposite. The proposition says that, provided that the hypotheses hold, this order relationship takes place if and only if the same relationship holds between the corresponding composite reflectances. Both facts are thus equivalent.

Finally, another version of proposition 9 which does not need estimates for L_d^c nor the NIR model, at the expense of not tolerating specularities, can be found below in the form of proposition 12: (As before, the proof is in [11, Appendix B].)

Proposition 12 *Assuming directional illumination is uniform throughout the scene and that ambient illumination is proportional to directional illumination, for any pair of colour channels c_1 and c_2 and any two image locations $p_1 = (i_1, j_1)$ and $p_2 = (i_2, j_2)$ such that $D_i^c(p_1) = 0$ and $D_i^c(p_2) = 0$,*

$$(1)\ \left.\begin{array}{l} D^{c_1}(p_1) > D^{c_2}(p_1) \\ D^{c_1}(p_2) < D^{c_2}(p_2) \end{array}\right\} \Leftrightarrow \left\{\begin{array}{l} C_b^{c_1}(p_1) > C_b^{c_2}(p_1) \\ C_b^{c_1}(p_2) < C_b^{c_2}(p_2) \end{array}\right. , \quad (2)\ \left.\begin{array}{l} D^{c_1}(p_1) < D^{c_2}(p_1) \\ D^{c_1}(p_2) > D^{c_2}(p_2) \end{array}\right\} \Leftrightarrow \left\{\begin{array}{l} C_b^{c_1}(p_1) < C_b^{c_2}(p_1) \\ C_b^{c_1}(p_2) > C_b^{c_2}(p_2) \end{array}\right.$$

- Proposition 10 provides the conditions which characterize a reflectance transition for which at least two channels are forced to evolve without coordination; that is to say, when the intensity in one increases, in the other one decreases (transition of type *non-coinciding derivative* or NCD). Analogously to proposition 9, the cases enumerated in proposition 10 correspond to the two ways how property 2 can be unsatisfied.

  On the other hand, notice that the formulation of proposition 10 does not make use of a derivative-like notation, unlike the corresponding property 2, but utilizes a notation based on two points $p_1 = (i_1, j_1)$ and $p_2 = (i_2, j_2)$ like the other two propositions. This is to elude the problem of the non-existence of intensity derivatives at reflectance transition locations.

  Observe that the proposition is written as a single implication. This is because the relationships between composite body reflectances expressed through the consequent of the proposition apply also to other cases where the colour channels do evolve in a coordinated way (see figure 3(a) for an illustration of this point). Therefore, both facts are not equivalent.

  Finally, notice that there is a certain degree of overlapping between CHC and NCD transitions. By

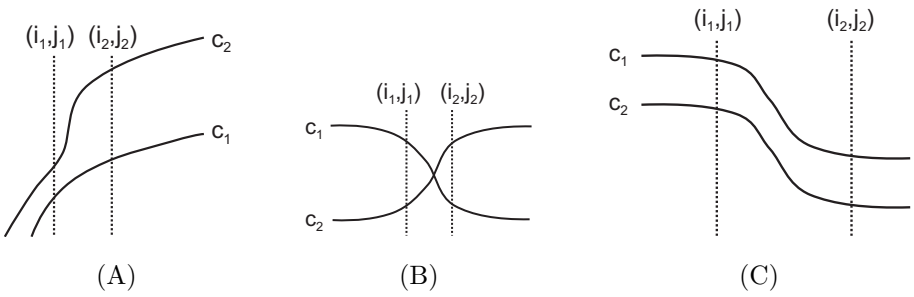

Fig. 3. (A) A case where possibly $\frac{C_b^{c_2}(p_1)}{C_b^{c_1}(p_1)} < \frac{C_b^{c_2}(p_2)}{C_b^{c_1}(p_2)}$, but $D^{c_1}(p_1) - D^{c_1}(p_2) < 0$ and $D^{c_2}(p_1) - D^{c_2}(p_2) < 0$. (B) A CHC and an NCD transition taking place simultaneously. (C) A case where possibly $C_b^{c_1}(p_1) > C_b^{c_1}(p_2)$ and $C_b^{c_2}(p_1) > C_b^{c_2}(p_2)$, but $D^{c_1}(p_1) \geq D^{c_1}(p_2)$, $D^{c_2}(p_1) \geq D^{c_2}(p_2)$, $D^{c_1}(p_1) \geq D^{c_2}(p_1)$, $D^{c_1}(p_2) \geq D^{c_2}(p_2)$, and $D^{c_1}(p_1) - D^{c_2}(p_1) \geq D^{c_1}(p_2) - D^{c_2}(p_2)$. $[p_1 = (i_1, j_1), p_2 = (i_2, j_2)]$

way of example, observe in figure 3(b) that every channel crossing implies two colour channels evolving without coordination during the reflectance transition. In case it was necessary to avoid the overlapping, an additional condition should be added to the two cases of proposition 10: $D^{c_1}(p_1) - D^{c_2}(p_1) \geq 0$ and $D^{c_1}(p_2) - D^{c_2}(p_2) \geq 0$, or $D^{c_1}(p_1) - D^{c_2}(p_1) \leq 0$ and $D^{c_1}(p_2) - D^{c_2}(p_2) \leq 0$.

- In the third place, proposition 11 characterizes a reflectance transition during which property 3 does not hold. Therefore, for at least two channels, the difference between their intensities does not decrease as the intensity in both decreases (transition of type *non-decreasing difference* or NDD). As can be seen, the formulation of proposition 11 is a bit special in the sense that the conditions that constitute the antecedents of the different implications include more terms than the conditions appearing in the formulation of property 3. This is because they are needed in the proof, although they also avoid a certain degree of overlapping between propositions 9/10 and proposition 11. In effect, by way of example, given $p_1 = (i_1, j_1)$ and $p_2 = (i_2, j_2)$, in case (1) of proposition 11, $D^{c_1}(p_1) \geq D^{c_1}(p_2)$ and $D^{c_2}(p_1) \geq D^{c_2}(p_2)$ are both needed simultaneously because, if they were not fulfilled at the same time, colour channels c_1 and c_2 would not evolve coordinately, and a transition of type NCD would have been found. Analogously, $D^{c_1}(p_1) \geq D^{c_2}(p_1)$ and $D^{c_1}(p_2) \geq D^{c_2}(p_2)$ are also necessary in order to ensure a transition of type CHC is not taking place. These two extra conditions do not appear in the formulation of property 3 because, as for every property both pixels (p_1) and (p_2) are assumed to have a common reflectance, $D^{c_1}(p_1) \geq D^{c_1}(p_2)$ implies $D^{c_1}(p_1) \geq D^{c_1}(p_2)$ (property 2) and $D^{c_1}(p_1) \geq D^{c_2}(p_1)$ implies $D^{c_1}(i_2,\, j_2) \geq D^{c_2}(p_2)$ (property 1).

  Finally, proposition 11 is not a double implication because, as in the case of proposition 10, the sort of reflectance transitions which are consequence of the conditions stated in the proposition can also arise due to other circumstances (see figure 3(c) for an illustration).

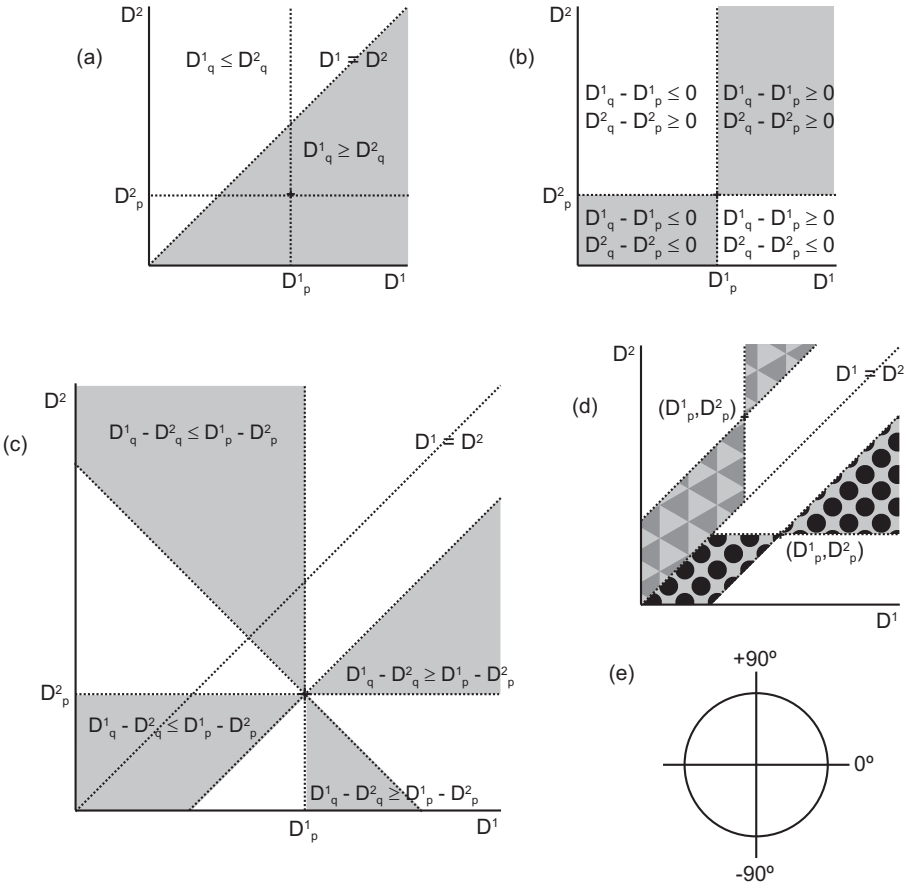

Fig. 4. Geometrical interpretation of properties 1-3. (In the figures, D_k^n is an abbreviation of $D_k^{c_n}$.)

7. Formulation of a Compatibility Relationship between Pixels

Properties 1-3 can be said to lead to a set of necessary compatibility conditions between pixels, in the sense that if two pixels fail to satisfy any of the three properties for any of the two-by-two combinations between colour channels, then both pixels cannot correspond to the same scene material. In this section, now that the usefulness of the aforementioned properties has been discussed, all three compatibility conditions will be unified in a single compatibility relationship between image pixels by means of their geometric interpretation. To simplify the explanation, a noiseless sensor will be considered first. Next, the relationship will be extended to noisy irradiance measurements.

7.1. *Geometric interpretation of properties 1-3 for noiseless irradiance measurements*

Given a certain combination of colour channels, say c_1 and c_2, and two pairs of intensity values, $(D_p^{c_1}, D_p^{c_2})$ and $(D_q^{c_1}, D_q^{c_2})$, all three properties can be stated geometrically considering the space of intensity values taken

by both channels:

- $(D_p^{c_1}, D_p^{c_2})$, with $D_p^{c_1} \geq D_p^{c_2}$, and $(D_q^{c_1}, D_q^{c_2})$ satisfy property 1 if and only if $D_q^{c_1} \geq D_q^{c_2}$. This is expressed in figure 4(a) as the shaded area below the straight line $D^{c_1} = D^{c_2}$; in other words, $(D_p^{c_1}, D_p^{c_2})$ with $D_p^{c_1} \geq D_p^{c_2}$ is compatible with any point $(D_q^{c_1}, D_q^{c_2})$ of the shaded area of figure 4(a) in the sense of property 1. In case $D_p^{c_1} \leq D_p^{c_2}$, the same order relationship must take place in the pair $(D_q^{c_1}, D_q^{c_2})$ for them to be compatible in the previous sense. This corresponds to the complement of the shaded area in figure 4(a). Notice that if $D_p^{c_1} = D_p^{c_2}$, any combination of intensity values for channels c_1 and c_2 is compatible with $(D_p^{c_1}, D_p^{c_2})$. This agrees with the aim of developing a set of necessary compatibility conditions, since, in this particular case, the pair $(D_p^{c_1}, D_p^{c_2})$ does not provide any clue about the order relationship between colour channels for the corresponding material, and therefore no reflectance transition should be suspected whatever $(D_q^{c_1}, D_q^{c_2})$ could be.
- $(D_p^{c_1}, D_p^{c_2})$ and $(D_q^{c_1}, D_q^{c_2})$ satisfy property 2 if intensity varies in the same sense for both channels from p to q: it increases in both, $D_p^{c_1} - D_q^{c_1} \geq 0$ and $D_p^{c_2} - D_q^{c_2} \geq 0$, or it decreases in both, $D_p^{c_1} - D_q^{c_1} \leq 0$ and $D_p^{c_2} - D_q^{c_2} \leq 0$. In figure 4(b), the shaded area include all the pairs $(D_q^{c_1}, D_q^{c_2})$ which verify these conditions for a certain $(D_p^{c_1}, D_p^{c_2})$. Observe that, in this case, the compatibility zone has nothing to do with the order relationship between colour channels.
- Finally, $(D_p^{c_1}, D_p^{c_2})$, with $D_p^{c_1} \geq D_p^{c_2}$, and $(D_q^{c_1}, D_q^{c_2})$ are such that an increase in intensity in one channel corresponds to an increase in the difference between colour channels, or, inversely, a decrease in intensity corresponds to a decrease in the difference (property 3) if:

(i) $D_q^{c_1} - D_q^{c_2} \geq D_p^{c_1} - D_p^{c_2}$ when $D_q^{c_1} \geq D_p^{c_1}$ and $D_q^{c_2} \geq D_p^{c_2}$ (upper right shaded area of figure 4(c)), or

(ii) $D_q^{c_1} - D_q^{c_2} \leq D_p^{c_1} - D_p^{c_2}$ when $D_q^{c_1} \leq D_p^{c_1}$ and $D_q^{c_2} \leq D_p^{c_2}$ (lower left shaded area of figure 4(c)), or

(iii) $D_q^{c_1} - D_q^{c_2} \leq D_p^{c_1} - D_p^{c_2}$ when $D_q^{c_1} \leq D_p^{c_1}$ and $D_q^{c_2} \geq D_p^{c_2}$ (upper left shaded area of figure 4(c)), or

(iv) $D_q^{c_1} - D_q^{c_2} \geq D_p^{c_1} - D_p^{c_2}$ when $D_q^{c_1} \geq D_p^{c_1}$ and $D_q^{c_2} \leq D_p^{c_2}$ (lower right shaded area of figure 4(c)).

As well as for property 1, in case $D_p^{c_1} \leq D_p^{c_2}$, the compatibility area is the complement of the shaded area of figure 4(c). For instance, if $D_q^{c_1} \geq D_p^{c_1}$ and $D_q^{c_2} \geq D_p^{c_2}$, property 3 holds if $D_q^{c_2} - D_q^{c_1} \geq D_p^{c_2} - D_p^{c_1}$ (upper right non-shaded area of figure 4(c)). When $D_p^{c_1} = D_p^{c_2}$, as before, the compatibility area is the whole space of values taken by channels c_1 and c_2.

To finish, observe that, contrary to the original formulation of property 3, this geometrical interpretation does not take into account properties 1 and 2. In fact, notice that cases (iii) and (iv) above violate property 2.

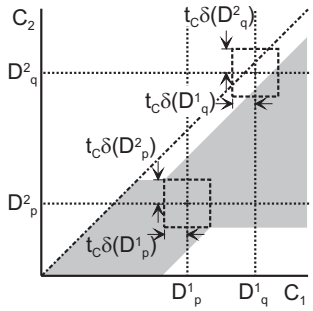

Fig. 5. Redefinition of the $\mathcal{C}$ compatibility relation. (The uncertainty areas have been magnified for illustration purposes. In the figure, D_k^n is an abbreviation of $D_k^{c_n}$.)

To finish, figure 4(d) shows the compatible area for all three properties simultaneously (triangles correspond to the case $D_p^{c_1} \leq D_p^{c_2}$, while circles are for case $D_p^{c_1} \geq D_p^{c_2}$). In view of these graphs, a compatibility relation $\mathcal{C}$ can be summarized as:

$(D_q^{c_1}, D_q^{c_2})$ *is* $\mathcal{C}$*-compatible with* $(D_p^{c_1}, D_p^{c_2})$ *if:*

(i) when $D_p^{c_1} \geq D_p^{c_2}$*, the orientation of the vector joining both lies within* $[0°, 45°]$*; and*

(ii) when $D_p^{c_1} \leq D_p^{c_2}$*, the orientation of the vector joining both lies within* $[45°, 90°]$.

This formulation of $\mathcal{C}$ assumes that the origin of the vector joining $(D_p^{c_1}, D_p^{c_2})$ and $(D_q^{c_1}, D_q^{c_2})$ is chosen so that its orientation lies between $-90°$ and $90°$ (see figure 4(e) for the angle convention).

7.2. *Extension to noisy irradiance measurements*

In order to counteract sensor noise in an adaptive way when applying relation $\mathcal{C}$, intensity uncertainties are considered. That is to say, for every colour channel c, every digital noisy level D^c produced by the camera is associated to an interval $[D^c - \delta(D^c), D^c + \delta(D^c)]$. To this end, algorithm R^{2}CIU [41] is used. R^{2}CIU computes intensity uncertainties on the basis of the camera noise model by Healey and Kondepudy [37]. With the introduction of these uncertainties, for a given $(D_p^{c_1}, D_p^{c_2})$, a rectangular uncertainty area around $(D_p^{c_1}, D_p^{c_2})$ covering t_C uncertainties is defined, as it is depicted in figure 5. $\mathcal{C}$ is then reformulated as:

$(D_q^{c_1}, D_q^{c_2})$ *is* $\mathcal{C}$*-compatible with* $(D_p^{c_1}, D_p^{c_2})$ *if any of the points belonging to the uncertainty area of* $(D_q^{c_1}, D_q^{c_2})$ *falls within the union of the compatibility zones of the points belonging to the uncertainty area of* $(D_p^{c_1}, D_p^{c_2})$ *(shaded area of figure 5).*

The incompatibility between $(D_p^{c_1}, D_p^{c_2})$ and $(D_q^{c_1}, D_q^{c_2})$ stems, thus, from the fact that a very low probability exists that any pair of intensity levels which could lead, through noise, to $(D_p^{c_1}, D_p^{c_2})$ was compatible, in the sense of properties 1-3, with any pair of intensity levels leading, through noise, to $(D_q^{c_1}, D_q^{c_2})$.

Finally, being $\delta(D^c)$ defined as indicated before, then, resorting to the Chebyshev inequality [2], $t_C = 2, 3$ and 4 represent that D^c will lie inside $[D^c - t_C\delta(D^c), D^c + t_C\delta(D^c)]$ with, respectively, probabilities of, at least, 75.00%, 88.89% and 93.75% [42]. If, besides, the different noise sources represented by $\delta(D^c)$ are approximated by Gaussians, the noise distribution results to be normal, and, therefore, the previous probabilities for $t_C = 2, 3$ and 4 increase, respectively, up to 95.45%, 99.73% and 99.99% (see [41]).

8. Coverage of Reflectance Transitions

The compatibility relationship $\mathcal{C}$ formulated before covers a broad spectrum of body reflectance changes. On the one hand, if property 1 is infringed, it is because at least one colour channel crosses one another. Otherwise, at that image pixel, colour channels do not cross one another, but, still, property 2 can be violated. In such a case, at least two colour channels diverge in the sense that, while in one channel the intensity increases, at the other one decreases. In case the intensity at all colour channels vary in a coordinated way —all increase or all decrease—, it can so happen that property 3 is not fulfilled; that is to say, when intensity decreases in both channels, the difference between them increases instead of decreasing, or vice versa.

Just to illustrate the broad coverage attained, CHC reflectance transitions comprise, from a theoretical point of view, the 83.33 % of all possible transitions (see [11, Appendix C] for the derivation of this percentage). What is most important from the previous fact is that $\mathcal{C}$ can be used to detect such an amount of reflectance transitions without resorting to explicitly computing the reflectance of the underlying surface.

However, unfortunately, there exist some reflectance transitions such that none of the cases of propositions 9-12 is fulfilled despite a reflectance change is arising there. These reflectance changes can be thought of as if the pixels involved corresponded all to the same scene material in the sense of not violating any of properties 1-3. Figures 3(a) and 3(c) are examples of this sort of reflectance transitions.

To investigate further this point, let us consider the situation of figure 3(a). As can be observed, all three properties are met in this case. More precisely, given $p_1 = (i_1, j_1)$ and $p_2 = (i_2, j_2)$:

[2] For a random variable $X(\mu, \sigma)$, $P(|X - \mu| \geq k\sigma) \leq 1/k^2, k > 0$.

$$D^{c_1}(p_1) < D^{c_1}(p_2)$$

$$D^{c_2}(p_1) < D^{c_2}(p_2)$$

$$D^{c_2}(p_1) > D^{c_1}(p_1) \Rightarrow D^{c_2}(p_1) - D^{c_1}(p_1) = (\alpha + m_b(p_1))\,(C_b^{c_2}(p_1) - C_b^{c_1}(p_1)) > 0$$

$$D^{c_2}(p_2) > D^{c_1}(p_2) \Rightarrow D^{c_2}(p_2) - D^{c_1}(p_2) = (\alpha + m_b(p_2))\,(C_b^{c_2}(p_2) - C_b^{c_1}(p_2)) > 0$$

$$D^{c_2}(p_1) - D^{c_1}(p_1) < D^{c_2}(p_2) - D^{c_1}(p_2)$$

$$\Rightarrow (\alpha + m_b(p_1))\underbrace{(C_b^{c_2}(p_1) - C_b^{c_1}(p_1))}_{>0} < (\alpha + m_b(p_2))\underbrace{(C_b^{c_2}(p_2) - C_b^{c_1}(p_2))}_{>0}$$

Observe that this last inequality can be satisfied under, among others, the two following sets of circumstances:

- $m_b(p_1) = m_b(p_2)$ and $C_b^{c_2}(p_1) - C_b^{c_1}(p_1) < C_b^{c_2}(p_2) - C_b^{c_1}(p_2)$, which means the changes in intensity $D^{c_1}(p_1) - D^{c_1}(p_2)$ and $D^{c_2}(p_1) - D^{c_2}(p_2)$ are due to a change in reflectance; or
- $m_b(p_1) < m_b(p_2)$, $C_b^{c_2}(p_1) = C_b^{c_2}(p_2)$ and $C_b^{c_1}(p_1) = C_b^{c_1}(p_2)$, which means the changes in intensity $D^{c_1}(p_1) - D^{c_1}(p_2)$ and $D^{c_2}(p_1) - D^{c_2}(p_2)$ are due to a change in the surface normal vectors.

Consequently, in this case, contrary to the situations depicted through propositions 9-12, there is no way to decide whether there is a change in reflectance or merely a change in m_b, and, thus, an ambiguity results. In other words, the interrelation between colour channels is not powerful enough in this case so as to disambiguate the source of the intensity variation. Notice that the analysis of images made so far is located at the signal level and, thus, the ambiguity lies at this level. Accordingly, information coming from the application domain level or from other sensor, if available, should be used to make the decision.

To illustrate the points addressed in this section, figures 6 and 7 show the $\mathcal{C}$-incompatibilities found for several real images. The map of incompatibilities shown was built by checking, at every pixel $p_1 = (i_1, j_1)$, whether for any of its 8 neighbours $p_2 = (i_2, j_2)$ and at least one combination of colour channels, both pixels were not compatible with one another in the sense of the relation $\mathcal{C}$ formulated in section 7.

As can be observed from the six images of figures 6 and 7, relationship $\mathcal{C}$ by itself is able to capture a considerable amount of reflectance transitions as predicted above, and, what is also relevant in many vision applications, with a very low cost both in time and computation resources. Notice that this is particularly true for the images of figure 6, above all for image (a).

Several other facts can also be observed from the images of figure 7. On the one hand, also as predicted before, those reflectance transitions that do not violate any of properties 1-3 are not detected (see, for instance, the reflectance transition corresponding to the pink and brown toys of image (a) of figure 7). On the other hand, when one of the objects intervening in the transition is dark or a shadow is involved, then the transition is not detected by $\mathcal{C}$ (see the backpack of image (b) of figure 7 as well as the reflectance

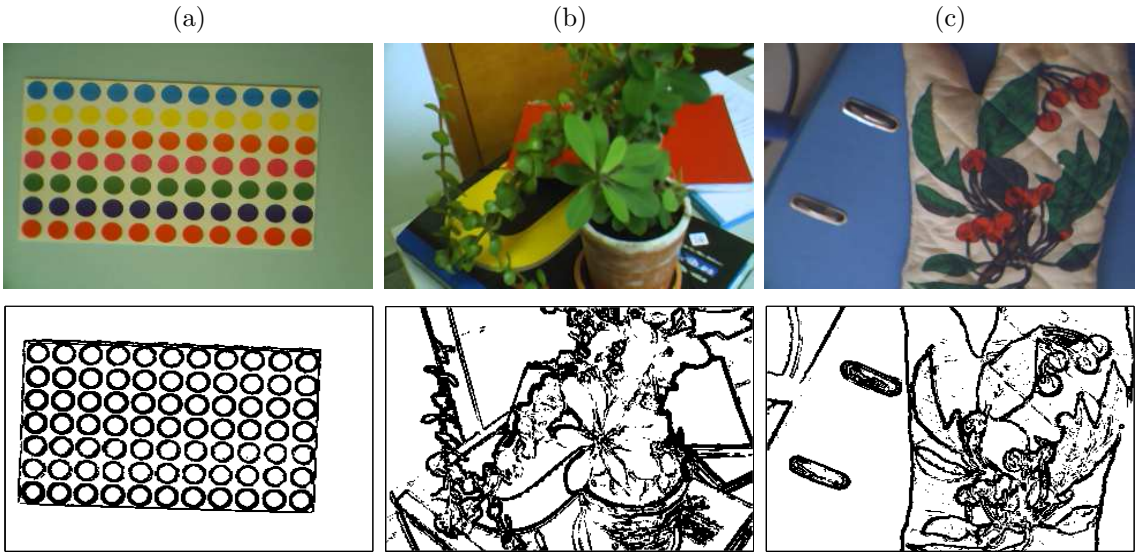

Fig. 6. Example of detection of $\mathcal{C}$-incompatibilities for real images (I): (1st row) original images; (2nd row) CHC/NCD/NDD transitions in black ($t_C = 3$).

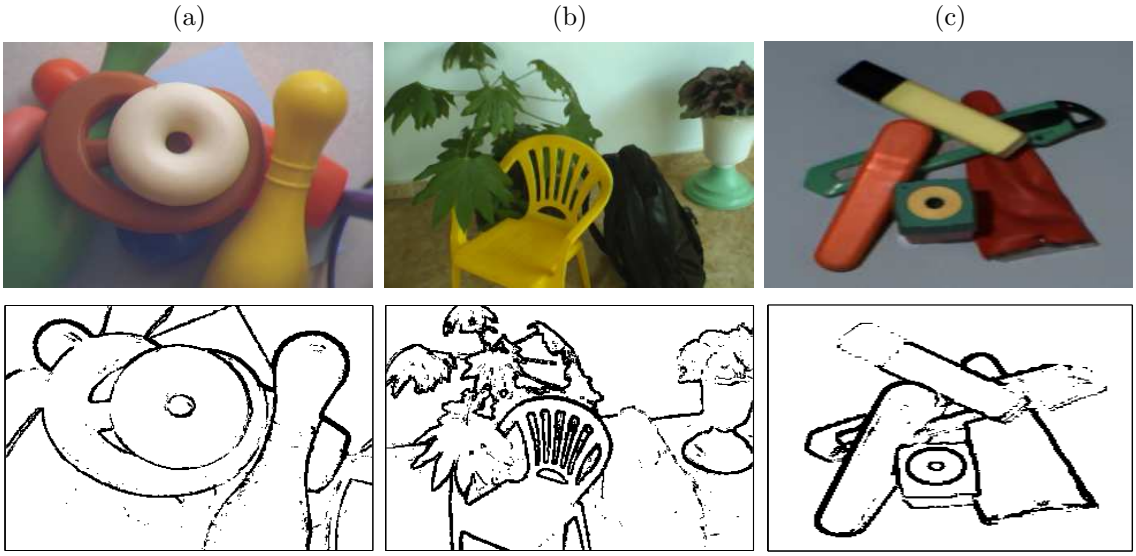

Fig. 7. Example of detection of $\mathcal{C}$-incompatibilities for real images (II): (1st row) original images; (2nd row) CHC/NCD/NDD transitions in black ($t_C = 3$).

transitions involving shadows). This is because the area of compatibility is large for low intensity values and, therefore, it is unlikely to find violations of properties 1-3.

Finally, reflectance transitions tend to span along more than two pixels in real images, what leads to "thick detections" of incompatibility (see figure 8), while in noiseless images, reflectance transitions should just involve two pixels. This lengthening of reflectance transitions is due to the round-off effect introduced by camera aliasing. Apart from rounding reflectance transitions off, it also has repercussions on the way

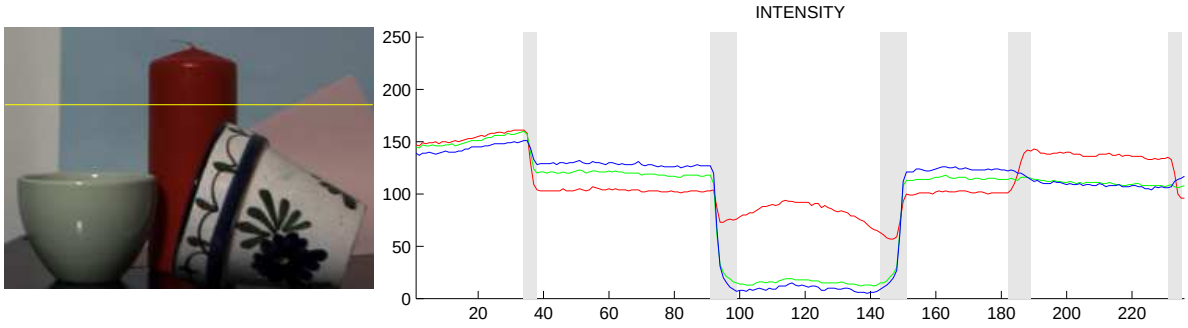

Fig. 8. Examples of reflectance transitions in a real image: intensity profiles for RGB colour channels, for row 50 (in yellow) of leftmost image (shadowed areas correspond to reflectance transition locations).

how intensity evolves during the change in reflectance. In effect, due to the different reflectance values at both sides of the transition for different pairs of channels, camera aliasing can produce asynchrony between colour channels in the sense that when the transition has finished in one channel it does not in the other. As a consequence of the aforementioned, the algorithm proposed before for analyzing the coupling between colour channels can have problems for dealing with small details (see, for instance, the text on the right of image (b) of figure 6).

From a global perspective, taking into account the previous images and many others, the incidence of the above-mentioned misbehaviours tends to be low, what proves that $\mathcal{C}$ is effective for detecting reflectance transitions in many situations with a very low cost. To cover all the possibilities, however, it is necessary to complement colour channel coupling analysis through $\mathcal{C}$ with additional detection means. Section 10 deals with this problem in order to develop an edge detector.

9. Relation with Similar Work

The coupling between colour channels which has been introduced in the preceding sections derives from the shape of the cluster constituted by the set of pixels corresponding to a uniformly coloured object in colour space. The DRM predicts that, in general, these pixels are confined within the parallelogram defined by the ambient $\boldsymbol{C_a}$, body $\boldsymbol{C_b}$ and interface $\boldsymbol{C_i}$ colour vectors (see equation 7); in case of a non-glossy object, the parallelogram reduces to the straight line defined by the ambient and the body colours. The coupling manifests, therefore, in the form of this confinement; that is to say, during the transition between neighbouring pixels, "jumping" outside the cluster is not allowed. This fact, although not explicitly mentioned, is exploited by many physics-based segmentation algorithms, either by the analysis of colour clusters or by means of photometric invariants (see [1–6], just to cite some of them).

10. Colour Channel Coupling-based Edge Detection (C^3E)

10.1. *General discussion*

As has been shown in the preceding sections, the analysis of the coupling between colour channels allows locating reflectance transitions. As this analysis is performed across the image, an edge map can be built, where every edge corresponds to a pixel involved in a reflectance change. As has also been shown, a small amount of reflectance transitions cannot be covered by means of relation $\mathcal{C}$, so that, in order to obtain a complete edge map, it is necessary to complement the previous analysis with additional means. For instance, if objects with smooth surfaces are expected in the scene, gradient information can result practical to locate the remaining reflectance transitions. They will be referred to as GRD reflectance transitions from now on.

Second-order derivative operators are of common use for edge detection in piecewise constant images. On those cases, the idealized step/ramp edges give rise to a zero crossing at the edge because of the sudden change in the first-order derivative, which in turn makes the second-order derivative change its sign in order to return to a situation of nearly zero gradient. In general images (i.e. in images where the intensity profiles are no longer piecewise constant but rather piecewise curved), zero-crossings occur at points where the image surface changes from being concave-shaped to be convex-shaped and vice versa. Although the inflection can happen in uniform reflectance areas as a consequence of the properties of the corresponding scene surface, it particularly occurs at reflectance transitions.

This section proposes a new edge detector called C^3E (*Colour Channel Coupling based Edge detection*) based on colour channel coupling which covers GRD reflectance transitions with the detection of LOG zero-crossings. In order to counteract image noise as well as $\mathcal{C}$ does, uncertainties are also introduced in this part of C^3E. More precisely, whenever a zero-crossing is detected, it is deemed relevant if the positive and negative peak LOG values along the direction of detection are larger than t_G times the respective uncertainties (see figure 9). The uncertainties are computed using standard uncertainty propagation rules, by which, if the output of the LOG operator is calculated as $f = \sum_x D^c(x)m(x)$, where $m(x)$ are the LOG mask constants, then [43]:

$$\delta(f) = \sqrt{\sum_x \delta(D^c(x))^2 m^2(x)} \tag{13}$$

(Notice that, being t_G defined in this way, its meaning is equivalent to the one for the parameter t_C introduced before.)

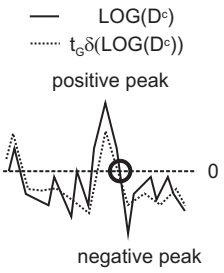

Fig. 9. Only the LOG zero-crossing behind the circle is considered relevant by C^{3}E.

10.2. *Edge map computation*

The edge map is computed according to the following procedure:

initialise *EdgeMap* to *NON_EDGE*

FOR $i = 1$ **TO** *NumberOfRows*

FOR $j = 1$ **TO** *NumberOfCols*

IF (i, j) is $\mathcal{C}$-incompatible with any of its 8 neighbours **THEN** $EdgeMap(i, j) = EDGE$

ELSE IF (i, j) is involved in a relevant LOG zero-crossing **THEN** $EdgeMap(i, j) = EDGE$

ENDIF

ENDFOR

ENDFOR

In this way, C^{3}E first verifies for every pixel whether there is a physical evidence of a reflectance transition arising there and only resorts to gradient information if there is no such a confirmation.

10.3. *Experimental Results*

To prove experimentally the usefulness of C^{3}E and by extension of colour channel coupling analysis, several results for synthetic and real images are provided in this section. Furthermore, for comparison purposes, results for the photometric-invariant-based edge detection algorithm by Stokman and Gevers [44, 45] (S&G from now on), as well as for the non-physics-based algorithm by Meer and Georgescu [46] (M&G from now on) are also given.

As for the parameters used in the different experiments:

– In the case of C^{3}E, the only relevant parameters are the number of uncertainties to be used when looking for $\mathcal{C}$-incompatibilities, t_C, and the number of uncertainties associated to GRD edges, t_G. The same value has been used for both, so that an only parameter results, which will be referenced as t. The value given to t in every experiment is indicated in each case.

Table 3
Some measures for evaluating the performance of edge detection algorithms.

measure	**formulation**	**typical values**
Pratt's FOM	$FOM(\alpha) = \frac{1}{\max\{n(A), n(B)\}} \sum_{x \in B} \frac{1}{1 + \alpha d(x, A)^2}$	$\alpha = 1$, $\alpha = 1/9$
Discrepancy Percentage	$D = \frac{n(A \Delta B)}{n(I)}$	—
Baddeley	$\Delta_w^p(A, B) = \sqrt[p]{\frac{1}{n(I)} \sum_{x \in I} \lvert w(d(x, A)) - w(d(x, B)) \rvert^p}$ $w(t) = \min\{t, c\}$	$p = 2, c = 5$

A is the set of image locations corresponding to edges in the reference edge map

B is the set of image locations corresponding to edges in the edge map under evaluation

I is the set of all image locations

$n(I)$ is the number of elements of set I

$A \Delta B = (A \setminus B) \bigcup (B \setminus A)$ (exclusive-or for sets)

$B \setminus A = \{x \in B | x \notin A\}$ (set minus operator for sets)

$d(x, Y)$ is the distance between image location x and the nearest edge in Y

On the other hand, the value of the standard deviation for the LOG operator, σ_{LOG} used for detecting GRD edges was all the time set to 1.0. The size of the LOG mask was then determined as $2 \times \lceil 3\sigma_{LOG} \rceil + 1$.

To finish with the particularities of the experiments involving C^{3}E, the edge maps are shown thinned. An edge thinning strategy based on the watershed transform has been used (see [11] for the details).

– Referring to S&G, it is a parameter-free algorithm which also uses intensity uncertainties to find local thresholds, so that no parameter needs to be set up. Besides, non-maxima suppression is used to thin the corresponding edge maps (as proposed by the authors) in order to have all the edge maps thinned throughout the algorithms comparison.

– Regarding M&G, the parameters set by default by the application they offer in their web page are used.

– Finally, up to four empirical discrepancy evaluation measures are provided in the comparisons among algorithms (see table 3): the often-cited Pratt's Figure of Merit (FOM) [47] with (1) $\alpha = 1/9$ and (2) $\alpha = 1$; (3) the discrepancy percentage (D), considered in Zhang's survey as one of the best discrepancy measures [48, 49]; and (4) the Baddeley measure [50], deemed the best evaluation technique in a recent survey [51]. All of them handle measures of discrepancy between a reference edge map and the output of the edge detector, although FOM and D yield values between 0 and 1, but Baddeley's measure between 0 and c. Furthermore, while Pratt's FOM scores good edge maps with larger values than bad edge maps, the percentage of discrepancy and Baddeley's measure both attain lower values with better edge maps.

10.3.1. *Experiments with synthetic images*

In the experiments with synthetic images, C^3E and S&G were faced against a set of 100 synthetic noisy images. Noise was added according to the noise model of Healey and Kondepudy [37] with the parameters estimated for a real camera using algorithm R^2CIU [41]. During the comparison, the level of noise corresponding to the real camera is called *normal noise conditions*, while *increasing noise conditions* means the standard deviations of the noise sources involved in the model are multiplied by a factor $k = 1..5$. On the other hand, the set consisted of scenes involving spheres and planes of different reflectances (see figure 10(top)).

Figure 10 provides the results of the comparison. As can be observed, Baddeley's measure indicates C^3E edge maps are better than the ones by S&G, under normal noise conditions (figure 10(middle)), while FOM and D measures are quite similar for both algorithms. The source of this discrepancy is likely to lay in the lack of sensitiveness to false edge positives of FOM [50]; as for the discrepancy percentage D, it should be taken into account that the location of misclassified pixels is not considered by this measure. On the other hand, the larger standard deviation of Baddeley's measure for S&G indicates a bigger instability of S&G against C^3E, although for some images S&G could have produced better edge maps than C^3E. As for increasing noise conditions, C^3E gets better scorings than S&G and, besides, C^3E shows a stronger tolerance to noise, with a performance similar to the one achieved under normal noise conditions (figure 10(bottom)).

10.3.2. *Experiments with real images*

This section presents experimental results for C^3E over a varied set of real images including images typically used for testing edge detection algorithms, i.e. standard images, and also "proprietary" images taken so as to ensure a linear relationship between image intensity and scene radiance according to equations 5 and 7 (this is required by physics-based vision algorithms in general).

Figure 11 and table 4 show comparison results for a set of real images for which a ground truth was manually generated. As can be noticed, C^3E outperforms S&G numerically in all cases, sometimes with a larger difference (figure 11(d)) and other times very slightly (figure 11(c)). As for M&G, C^3E tends also to produce better edge maps, although, on some occasions, the numerical values are almost the same. The larger differences in performance between physics and non-physics-based algorithms appear, as could be easily guessed, for images containing curved objects (figures 11(a) and (b)). Observe that M&G produces edges related with scene curvature while C^3E does not because of its basis on the physics of image formation. For instance, see the green cup of the image in figure 11(a). However, in the same image, it can be noticed that C^3E does not deal with small details as well as M&G, as can be observed in the ornamentation of

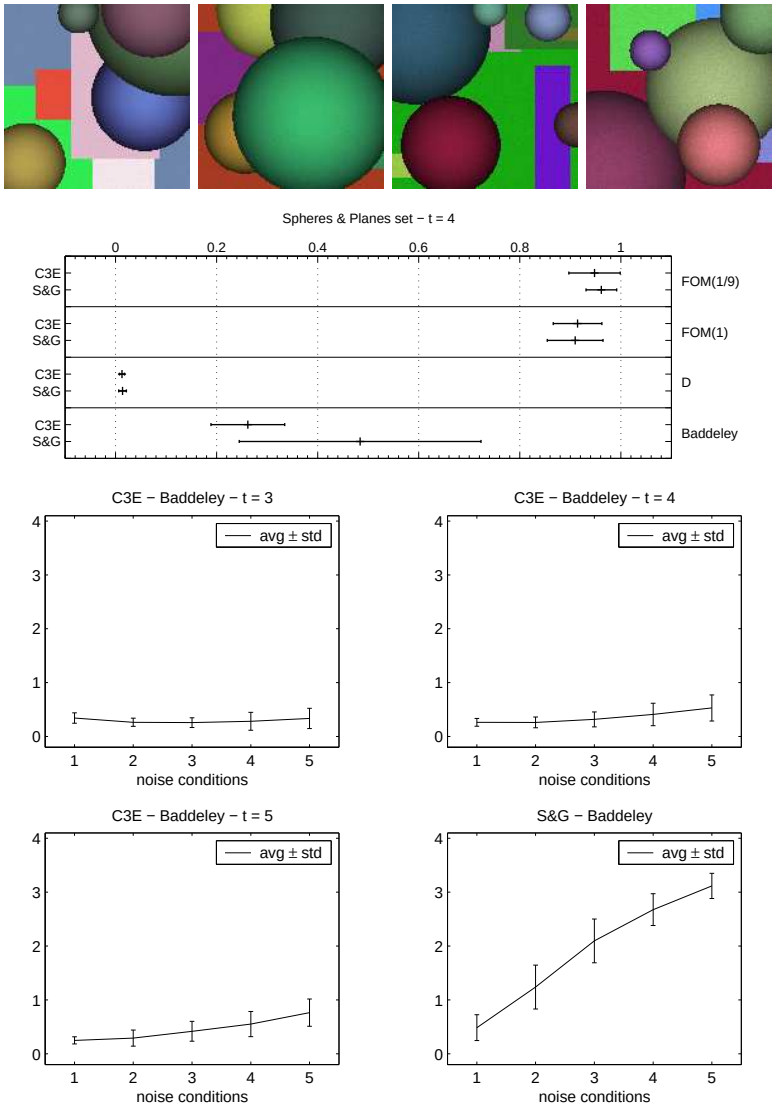

Fig. 10. Comparison between C^{3}E and S&G under noisy conditions by means of synthetic images: (top) examples of noisy synthetic images; (middle) normal noise conditions, the plots show average and standard deviation values for $t = 4$; (bottom) increasing noise conditions, the plots show average and standard deviation of Baddeley's measure for $t = 3..5$.

the upper part of the flowerpot of figure 11(a). Clearly, the contours are better delineated by M&G. This behaviour has to do with the fact that C^{3}E labels as edges all the pixels involved in a reflectance transition and, thus, thick edges result which are not properly thinned in the thinning stage, what makes difficult the treatment of details of reduced size. The obvious solution for these cases is, of course, to increase image resolution. Finally, notice that, for some images, M&G produces better edge maps than S&G. However, this happens more notoriously with the standard images, for which, surely, gamma correction was not turned off, what can affect S&G (and also C^{3}E).

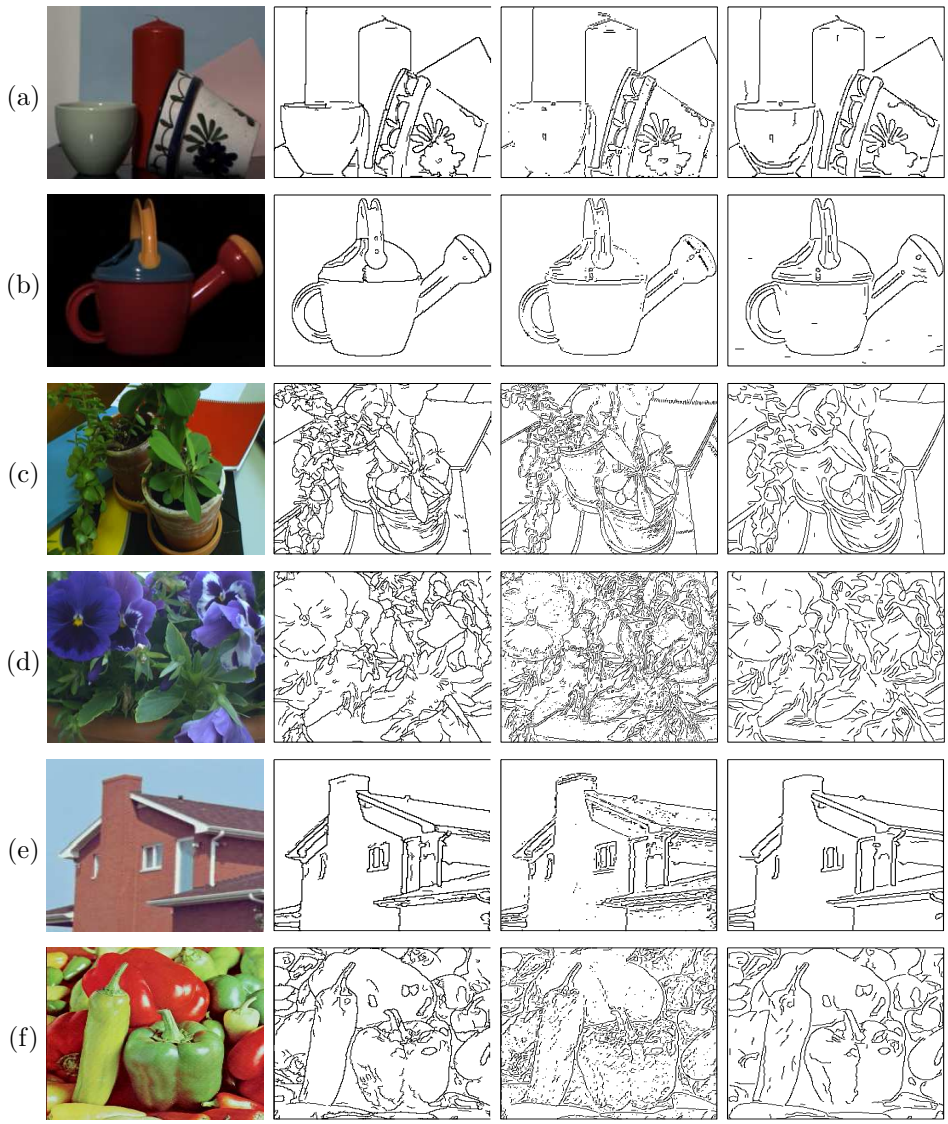

Fig. 11. Edge maps for real images on the left: (2nd col) C^3E and $t = 4$; (3rd col) S&G; (4th col) M&G.

11. Conclusions

This paper has investigated colour channel coupling from a physics-based viewpoint. As has been shown, colour channels keep coupled in uniform reflectance areas, while the coupling is broken in a number of ways at pixels involved in reflectance transitions. This coupling has been expressed in the form of a set of properties which are fulfilled by all the pixels corresponding to the same surface material (i.e. same reflectance), so that, when any of them is not satisfied, the only possible cause of the unfulfillment reduces to a change in reflectance. The satisfaction of those properties has been studied for different instantiations of the image formation model, what has allowed determining, from a theoretical point of view, the constraints to be met

Table 4
Comparison between C^3E, S&G and M&G with the real images of figure 11. In the table, $F_{\frac{1}{9}} \equiv$ FOM(1/9), $F_1 \equiv$ FOM(1), %D $\equiv$ D $\times$100, B $\equiv$ Baddeley.

		C^3E			S&G	M&G			C^3E			S&G	M&G
		$t=3$	$t=4$	$t=5$					$t=3$	$t=4$	$t=5$		
(a)	$F_{\frac{1}{9}}$	0.68	0.65	0.62	0.56	0.58	(d)	$F_{\frac{1}{9}}$	0.52	0.56	0.60	0.44	0.47
	F_1	0.62	0.59	0.57	0.51	0.51		F_1	0.38	0.42	0.46	0.28	0.33
	%D	6.21	6.15	6.20	6.78	7.79		%D	13.88	12.20	10.99	18.57	13.82
	B	0.75	0.75	0.78	0.82	1.13		B	2.22	2.03	1.89	2.73	2.32
(b)	$F_{\frac{1}{9}}$	0.73	0.71	0.69	0.59	0.64	(e)	$F_{\frac{1}{9}}$	0.88	0.88	0.86	0.80	0.70
	F_1	0.55	0.54	0.53	0.42	0.46		F_1	0.70	0.73	0.71	0.58	0.58
	%D	5.17	5.03	4.87	5.47	5.83		%D	6.59	6.05	6.05	8.80	6.02
	B	0.97	0.90	0.85	1.08	1.22		B	0.80	0.66	0.71	1.15	0.78
(c)	$F_{\frac{1}{9}}$	0.69	0.70	0.72	0.67	0.64	(f)	$F_{\frac{1}{9}}$	0.47	0.53	0.56	0.46	0.54
	F_1	0.52	0.53	0.56	0.47	0.48		F_1	0.35	0.41	0.44	0.30	0.43
	%D	12.67	12.23	11.50	14.04	12.28		%D	12.67	10.56	9.42	13.71	9.04
	B	1.69	1.64	1.56	1.73	1.78		B	2.30	2.01	1.86	2.48	1.87

by the scene so that these properties can be effectively used to locate reflectance transitions. An important aspect of the analysis proposed is that it does not depend on the particular expression selected for the different terms of the DRM: m_b and m_i — non-spectral (geometrical) terms —, and $L_d(\lambda)\rho_b(p;\lambda)$ and $L_d(\lambda)\rho_i(p;\lambda)$ — spectral terms—, see equation 7. Besides, the geometrical interpretation of the aforementioned properties has allowed defining a very-easy-to-check compatibility relationship $\mathcal{C}$ between pixels which allows determining with very low cost whether they share the same reflectance or not.

As an example of application of the proposed colour channel coupling analysis, a very low-cost new edge detector named C^3E (*Colour Channel Coupling-based Edge detection*) based on $\mathcal{C}$ has been presented. The following conclusions can be drawn from the different experiments performed, showing the power of the coupling analysis for locating reflectance transitions in general scenes, i.e. scenes containing curved objects and different surface materials:

– The scene constraints concerning the fulfillment of the coupling properties have not been a serious problem for obtaining sound edge maps.
– C^3E does not show important differences between scenes where objects shading is noticeable with regard to scenes where it is not. Three or four uncertainties are enough to produce adequate edge maps on most occasions.
– C^3E has exhibited a good tolerance to noise.
– Finally, C^3E has compared well with the photometric-invariant-based edge detection algorithm by Stokman and Gevers [44, 45] (S&G) and with the recognized non-physics-based edge detection algorithm by Meer and Georgescu [46] (M&G).

Acknowledgements

This study has been partially supported by project CICYT-DPI2005-09001-C03-02 and FEDER funds.

References

[1] T. Gevers, Adaptive image segmentation by combining photometric invariant region and edge information, IEEE Transactions on Pattern Analysis and Machine Intelligence 24 (6) (2002) 848–852.

[2] T. Gevers, A. W. Smeulders, H. Stokman, Photometric invariant region detection, in: Proceedings of the British Machine Vision Conference, 1998, pp. 659–668.

[3] G. J. Klinker, S. A. Shafer, T. Kanade, A physical approach to color image understanding, International Journal of Computer Vision 4 (1) (1990) 7–38.

[4] C.-K. Ong, T. Matsuyama, Robust color segmentation using the dichromatic reflection model, in: Proceedings of the IEEE International Conference on Pattern Recognition, 1998, pp. 780–784.

[5] A. Ortiz, G. Oliver, A qualitative approach to physics-based image segmentation, in: Proceedings of Advanced Concepts for Intelligent Vision Systems, 2002.

[6] A. Ortiz, G. Oliver, A method to discount ambient lighting and albedo variation before estimating shape from image shading, in: Proceedings of Advanced Concepts for Intelligent Vision Systems, 2002.

[7] Y. Ohta, T. Kanade, T. Sakai, Color information for region segmentation, Computer Graphics and Image Processing 13 (3) (1980) 222–241.

[8] G. E. Healey, Segmenting images using normalized color, IEEE Transactions on Systems, Man and Cybernetics .

[9] T. Gevers, H. Stokman, Robust histogram construction from color invariants for object recognition, IEEE Transactions on Pattern Analysis and Machine Intelligence 26 (1) (2004) 113–117.

[10] S. A. Shafer, Using color to separate reflection components, COLOR Research and Application 10 (4) (1985) 210–218.

[11] A. Ortiz, New segmentation and edge detection methods using physics-based models of image formation, Ph.D. thesis, University of the Balearic Islands, (Available online at http://dmi.uib.es/~aortiz/AORthesis.zip) (2005).

[12] R. Hall, Illumination and color in computer generated imagery, Springer-Verlag, 1989.

[13] J. Birn, Digital Lighting and Rendering, New Riders Publishing, 2000.

[14] H. W. Jensen, Realistic Image Synthesis Using Photon Mapping, AK Peters, 2001.

[15] S. Tominaga, B. A. Wandell, Standard surface-reflectance model and illuminant estimation, Journal of the Optical Society of America - A 6 (4) (1989) 576–584.

[16] S. Tominaga, Surface Identification Using the Dichromatic Reflection Model, IEEE Transactions on Pattern Analysis and Machine Intelligence 13 (7) (1991) 658–670.

[17] H.-C. Lee, E. J. Breneman, C. P. Schulte, Modeling light reflection for computer color vision, IEEE Transactions on Pattern Analysis and Machine Intelligence 12 (4) (1990) 402–409.

[18] G. E. Healey, Using color for geometry-insensitive segmentation, Journal of the Optical Society of America - A 6 (6) (1989) 920–937.

[19] J. Reichman, Determination of absorption and scattering coefficients for nonhomogeneous media. 1: Theory., Applied Optics 12 (1973) 1811–1815.

[20] S. Tominaga, Dichromatic reflection models for a variety of materials, COLOR Research and Application 19 (4) (1994) 277–285.

[21] S. Tominaga, Dichromatic reflection models for rendering object surfaces, Journal of Imaging Science and Technolog 40 (6) (1996) 549–555.

[22] T. Hashimoto, H. Kato, K. Sato, S. Inokuchi, , K. Moriwaki., Recognition of material types and interreflection using color images, Systems and Computers in Japan 23 (12) (1992) 727–735.

[23] M. Oren, S. K. Nayar, Generalization of the Lambertian model and implications for machine vision, International Journal of Computer Vision 14 (3) (1995) 227–251.

[24] L. B. Wolff, A diffuse reflectance model for smooth dielectrics, Journal of the Optical Society of America - A 11 (11) (1994) 2956–2968, (special issue on Physics Based Machine Vision).

[25] L. B. Wolff, S. K. Nayar, M. Oren, Improved diffuse reflection models for computer vision, International Journal of Computer Vision 30 (1) (1998) 55–71.

[26] K. Torrance, E. Sparrow, Theory for off-specular reflection from roughened surfaces, Journal of the Optical Society of America 57 (1967) 1105–1114.

[27] P. Beckmann, A. Spizzichino, The Scattering of Electromagnetic Waves from Rough Surfaces, Macmillan, New York, 1963.

[28] R. Cook, K. Torrance, A reflectance model for computer graphics, Computer Graphics 15 (1981) 307–316.

[29] G. E. Healey, T. O. Binford, Local shape from specularity, Computer Vision, Graphics, and Image Processing 42 (1988) 62–86.

[30] B. Phong, Illumination for computer generated pictures, Communications of the ACM 18 (1975) 311–317.

[31] G. Ward, Measuring and modeling anisotropic reflection, in: Proceedings of SIGGraph, 1992, pp. 265–272.

[32] H. Tagare, R. de Figueiredo, A framework for the construction of reflectance maps for machine vision, Computer Vision, Graphics, and Image Processing 57 (3) (1993) 265–282.

[33] R. C. Love, Surface reflection model estimation from naturally illuminated image sequences, Ph.D. thesis, School of Computer Studies, University of Leeds (1997).

[34] S. Tominaga, N. Tanaka, Estimating reflection parameters from a single color image, IEEE Computer Graphics and Applications 20 (5) (2000) 58–66.

[35] R. Gershon, A. D. Jepson, J. K. Tsotsos, Ambient illumination and the determination of material changes, Journal of the Optical Society of America - A 3 (10) (1986) 1700–1707.

[36] C. L. Novak, S. A. Shafer, Color vision, in: Encyclopedia of Artificial Intelligence, J. Wiley and Sons, 1992, pp. 192–202.

[37] G. E. Healey, R. Kondepudy, Radiometric CCD camera calibration and noise estimation, IEEE Transactions on Pattern Analysis and Machine Intelligence 16 (3) (1994) 267–276.

[38] B. Horn, R. Sjoberg, Calculating the reflectance map, Applied Optics 18 (11) (1979) 1770–1779.

[39] F. Perez, C. Koch, Toward color image segmentation in analog VLSI: algorithm and hardware, International Journal of Computer Vision 12 (1) (1994) 17–42.

[40] W. H. Tsang, P. W. M. Tsang, Suppression of false edge detection due to specular reflection in color images, Pattern Recognition Letters 18 (2) (1997) 165–171.

[41] A. Ortiz, G. Oliver, Radiometric calibration of vision cameras and intensity uncertainty estimation, Image and Vision Computing 24 (10) (2006) 1137–1145, (Available online 30 june 2006).

[42] B. W. Lindgren, Statistical Theory, 4th Edition, Chapman & Hall, 1993.

[43] J. R. Taylor, An Introduction to Error Analysis, 2nd Edition, University Science Books, 1997.

[44] T. Gevers, H. Stokman, Classifying color edges in video into shadow-geometry, highlight, or material transitions, IEEE Transactions on Multimedia 5 (2) (2003) 237–243.

[45] H. Stokman, Robust Photometric Invariance in Machine Colour Vision, Ph.D. thesis, Intelligent Sensory Information Systems Research Group - Faculty of Science (University of Amsterdam) (2000).

[46] P. Meer, B. Georgescu, Edge detection with embedded confidence, IEEE Transactions on Pattern Analysis and Machine Intelligence 23 (12) (2001) 1351–1365, (The code is publicly available at http://www.caip.rutgers.edu/riul/research/code.html).

[47] W. Pratt, Digital Image Processing, 2nd Edition, John Wiley and Sons, 1991.

[48] Y. Zhang, A survey on evaluation methods for image segmentation, Pattern Recognition 29 (8) (1996) 1335–1346.

[49] R. Roman-Roldan, J. Gomez-Lopera, C. Atae-Allah, J. Martinez-Aroza, P. Luque-Escamilla, A measure of quality for evaluating methods of segmentation and edge detection, Pattern Recognition 34 (5) (2001) 969–980.

[50] A. Baddeley, An error metric for binary images, in: W. Förstner, S. Ruwiedel (Eds.), Robust Computer Vision: Quality of Vision Algorithms, Wichmann, Karlsruhe, 1992, pp. 59–78, (Proceedings of the International Workshop on Robust Computer Vision).

[51] N. Fernandez-Garcia, R. Medina-Carnicer, A. Carmona-Poyato, F. Madrid-Cuevas, M. Prieto-Villegas, Characterization of empirical discrepancy evaluation measures, Pattern Recognition Letters 25 (1) (2004) 35–47.